Received: 26 March 2024 | Revised: 28 June 2024 | Accepted: 6 July 2024

DOI: 10.1002/cta.4196

ORIGINAL ARTICLE

WILEY

Enhancing damping of low-frequency oscillations in power networks through energy storage system-based controller

Rohit Kumar | **Soumya R. Mohanty** | **Mitresh Kumar Verma**

Department of Electrical Engineering, Indian Institute of Technology (BHU), Varanasi, India

Correspondence
Rohit Kumar, Electrical Engineering Department, Indian Institute of Technology (BHU), Varanasi 221005, India.
Email: rohit.kumar.rs.eee18@itbhu.ac.in

Summary

Mitigating inter-area low-frequency oscillations is a significant concern in multi-machine power systems due to their adverse effects on system stability. These oscillations are intricately linked with power oscillations. So appropriate power modulation through the Battery Energy Storage System (BESS) can be an effective strategy for preserving system stability. In this paper, the maximal of all minimal residue indices under variations in power system operating conditions is utilized as the index for identifying the location for installation of the BESS, the damping control loop, and the feedback signal. A fixed-structure H_∞ scheme-based wide-area damping controller (WADC) is proposed for the BESS, providing sufficient damping of inter-area oscillation modes. A modified IEEE 39-bus system is simulated using a real-time digital simulator as a test system in this work. The simulation results confirmed that the proposed WADC could effectively damp various inter-area oscillation modes. Furthermore, it offers robust damping performance over contingencies associated with the system's various operating scenarios as well as the uncertainty associated with fixed and variable communication delays in the feedback signal of WADC and the integration of solar photovoltaic systems. Moreover, a comparative analysis of the proposed WADC is carried out with a BESS-based wide-area power system stabilizer, which is found to be more effective in mitigating system inter-area oscillations.

KEYWORDS

battery energy storage system, damping control loop, fixed-structure H_∞ controller, inter-area oscillation, operating scenarios, RTDS

1 | INTRODUCTION

1.1 | Background

A major problem in modern power systems is transferring large amounts of power across long transmission lines from one region to another due to rising power demand. In order to improve the transient stability of the power system, nonlinear components such as fast automatic voltage regulators are frequently being integrated. On the other hand, incorporating such devices gives rise to developing low-frequency oscillations (LFOs) at frequencies below 2 Hz,[1] which are sustained in the system. When synchronous generators (SGs) oscillate against one another at a frequency of 1–2 Hz in a single geographical area, local oscillation modes are triggered in a power system. On the other hand, inter-area oscillation modes are observed when a set of SGs in one area swings against a group of SGs in another area. The LFOs are detrimental and must be damped out as soon as possible to keep the system stable and reliable.

Consequently, power system stabilizers (PSSs) are used in multi-machine systems to enhance the comprehensive damping for the local oscillation mode of SG rotor oscillations by employing supplemental stabilizing signals. Conventional lead–lag PSSs employ the phase compensation method, which may require parameter adjustments for widespread operating scenarios. To address these challenges, Liu et al.[2] introduces a heuristic-dynamic programming-based solution for phase compensation-based PSSs. Nevertheless, these controllers might not adequately damp inter-area oscillation modes due to the limited observability of local signals.[3] These inter-area modes, often weakly damped and dominant, necessitate efficient damping to ensure consistent power transfer. Within this context, energy storage systems (ESSs) play a significant role in substantially enhancing power system reliability. In,[4] using an energy storage device with optimal feedback control schemes is suggested to improve power dynamic performance, encompassing enhanced power flow through inter-area lines and effective frequency regulation during varying loading conditions. So, this study proposed the fixed-structure H_∞ control-based Wide-Area Damping Controller (WADC) for Battery Energy Storage Systems (BESS) to alleviate power system LFOs under the change in system operating conditions.

1.2 | Literature review

Existing research has investigated various strategies for mitigating the power system LFOs, predominantly utilizing local signals in the design of damping controllers. However, these local signals often lack the necessary observability for addressing inter-area modes effectively. In such scenarios, the design of damping controllers for inter-area oscillations leans towards preferring wide-area feedback signals. Addressing the prior concern of limited observability in local signals, incorporating wide-area signals from phasor measurement units (PMUs) introduces a challenge, as these signals inherently experience communication time delay that might adversely impact the performance of WADC. The time delay duration is impacted by network distance, communication link type, transmission protocols, and more, potentially spanning tens to several hundreds of milliseconds.[5] Thus, considering time delay in feedback signals becomes vital in WADC design. The Padé approximation[6] is frequently employed as the prevailing approach to address time delays, often involving the consideration of a fixed first or second-order time delay.

Moreover, the proposed scheme in Beiraghi and Ranjbar[7] suggests adaptive delay compensators to mitigate communication time delay effects on WADC. However, these schemes necessitate additional components linked with the WADC, leading to increased system complexity and cost. In contrast, this work eliminates the requirement for a dedicated time delay compensator. The WADC design process here inherently encompasses the potential minimum and maximum communication time delay limits within the feedback control loop, thus providing the WADC with inherent robustness to time delays. As a result, it diminishes the total cost of the proposed WADC scheme.

Existing literature offers numerous techniques for designing WADC that will reduce inter-area oscillations in the power system. The wide-area PSS is proposed in Prakash et al.,[5] with its parameters fine-tuned using hybrid algorithms like teacher-learner-based optimization and particle swarm optimization. The WADC scheme based on Bellman's principle and the Loewner Interpolation Method is presented in Paternina et al.[8] to mitigate LFOs in power systems. A coordinated approach-based WADC for wind generation is outlined in Kumar and Bhadu,[9] with the WADC parameters optimized using the multi-objective gray wolf optimizer algorithm. The wide-area output feedback controller is presented in Alghamdi et al.[10] that takes into account time-varying delays for converter-based resources and conventional generators, thereby enhancing oscillation damping in a low-inertia power network. The concept of harnessing coherent group generators for designing WADC is presented in Naguru[11] for an integrated power network. Further, multipliers-based WADC is established in Thakallapelli and Kamalasadan,[12] as is a WADC alternating direction technique. This method relies on coherency grouping, in which the entire power system is separated into several areas and then constructed using a residue-based strategy. Nevertheless, it's worth highlighting that the application of these damping controllers lacks validation on large power networks that exhibit several LFO modes.

The WADC technique proposed in Zenelis and Wang,[13] based on a modal linear quadratic regulator control scheme, simultaneously improves power system LFOs' damping. The time-delayed feedback control approach-based WADC for solar photovoltaic systems is presented in Kumar et al.[14] to alleviate the power system LFOs. Furthermore, the H_∞ damping controllers are the most extensively used controllers for suppressing the inter-area oscillation modes, as suggested in Banerjee et al.[15] The power system LFO mode damping enhancement through location and controller parameters for BESSs are optimized using the mixed-PSO technique presented in Zhu et al.[16] The capacitive ESS, associated with a fractional-order proportional tilt integral derivative plus one controller, is discussed in Choudhary et al.[17] to control the power system frequency and mitigate the power required by load fluctuations. Moreover, a resilient WADC utilizing a multiple-controller switching scheme is presented in Zhao et al.[18] to suppress the cyber attack on the power system network and enhance damping in inter-area modes.

1.3 | Research gap and motivation

The existing literature lacks a clear understanding of the appropriate location for deploying BESS into multi-machine power networks to mitigate system LFOs and enhance system stability effectively. The appropriate location of a BESS in a multi-machine power system is essential for enhancing the damping performance of inter-area oscillations. Proper placement ensures that the BESS can manage power flows, effectively stabilize the system, and synchronize with other control mechanisms, thereby improving overall system reliability and stability. Additionally, there is a notable absence of discussion regarding selecting an effective damping control loop of BESS, such as an active power control loop or reactive power control for installing the supplementary damping controller. The current literature also lacks a comprehensive investigation into the design of damping controllers for BESS-integrated power systems, particularly in wide-area scenarios involving various system uncertainties. These uncertainties include variable communication delays in the feedback loop, nonlinearities in the damping control loop, and the integration of renewable sources such as solar PV systems. Hence, this study aims to address these gaps by utilizing BESS as an actuator to mitigate system LFOs across diverse operating conditions scenarios because it can provide both active and reactive power support with high precision and speed. This dual capability enhances the damping of power system oscillations, including local and inter-area modes, thereby improving overall system stability.

1.4 | Challenges

Designing a fixed-structure H_∞ control-based WADC for BESS to alleviate power system LFOs presents significant challenges. These include accurately capturing the complex dynamics of wide-area power systems, managing uncertainties in system parameters and communication delays, and integrating BESS effectively into the control framework.

1.5 | Contribution

In this paper, the dynamics of the DC-to-DC bidirectional converter, along with the DC voltage controller, and the dynamics of the VSC associated with primary and secondary control loops, such as power and current control loops, are included in the modeling stage of BESS to analyze the impact of system LFOs. Furthermore, the appropriate placement of BESS in the power system and the suitable control loop, whether active or reactive power control, for placing the damping controller are determined using modal analysis, respectively. A reduced-order model-based fixed-structure H_∞ scheme-based WADC is proposed to enhance the damping performance for system LFOs. The damping performance of the proposed WADC is validated under different operating conditions and various uncertainties, including variable and fixed communication delays in the feedback signal of the damping controller and the penetration of renewable energy sources into the system. In these contexts, the following are the main contributions of this article:

1. The application of BESS in multi-machine power systems in the context of frequency stability and oscillation damping, as discussed in Calero et al.[19] and Datta et al.,[20] does not discuss the appropriate location of BESS to integrate into the system. As a result, in this paper, the selection strategy for determining the appropriate BESS placement in the power system is based on the maximum of all minimal residue indices using modal analysis under varying system loading conditions. This strategy is employed to choose the best location for the BESS, the appropriate feedback signal, and the suitable damping control loop (i.e., active or reactive power control) for placing a supplementary damping controller.

2. A fixed-structure H_∞ scheme-based WADC is proposed for BESS to mitigate power system inter-area oscillations. The robustness of this control scheme is verified against several system contingencies. These include different loading conditions, various fault locations, uncertainties related to the nonlinearity in the output of the damping controller, integration of renewable sources, and communication time delays (fixed and variable) in the feedback loop.
3. In this study, we conducted an extensive simulation analysis to thoroughly evaluate the impact of the proposed WADC on the system's damping performance. Our investigation specifically focused on understanding how the WADC, when interconnected with the active and reactive control loops of the BESS, affects the damping characteristics of the system across different operating scenarios.

1.6 | Paper organization

The remaining sections of this work are structured as follows: Section 2 discusses power system modeling, BESS modeling, and small-signal analysis. The BESS selection approach is covered in Section 3. Section 4 discusses the design of the proposed fixed-structure WADC for BESS. The proposed method is verified on the modified New England 10-machine benchmark system in Section 5. Moreover, real-time validation is carried out on real-time digital simulator (RTDS) in Section 6. Lastly, Section 7 concludes this work.

2 | POWER SYSTEM MODELING

This study delves into the impact of BESS and BESS-based WADC on the inter-area oscillation modes within a multi-machine power system. The power system comprises essential components such as SGs, exciters, local PSS, transmission networks, and loads. Each SG is represented as a 6th-order sub-transient model equipped with an IEEE Type I excitation system and a Type I governor. Transmission networks and loads are modeled using Π models and constant impedance, respectively. The forthcoming subsection provides a detailed discussion of BESS modeling.

2.1 | BESS model

The BESS integrated into the power system comprises the battery pack, power conditioning system (PCS), filter, and transformer. The PCS is a group of power converters that work together to keep the power and voltage output at the desired levels. The PCS for the BESS consists of a DC-to-DC bidirectional converter for battery charging/discharging control and a voltage source converter (VSC) for power network integration with required power output and voltage. The elaborate block diagram structure of BESS with the associated controller is shown in Figure 1.

2.1.1 | Battery pack model

The DC-to-DC converter connects the battery cells in the battery pack module in series and parallel to produce the desired power and voltage. The battery is represented as a controlled DC source in series with an internal resistance R_b based on the generic model.[21]

2.1.2 | DC-to-DC bidirectional converter model

In this study, the average model of a bidirectional converter in discharging mode operate in discontinuous conduction mode, and the magnitude of the DC-link current represents the VSC load I_{dc}. The weighted average dynamics model of the bidirectional converter in discharging mode across the switching period T_C is written as[22]

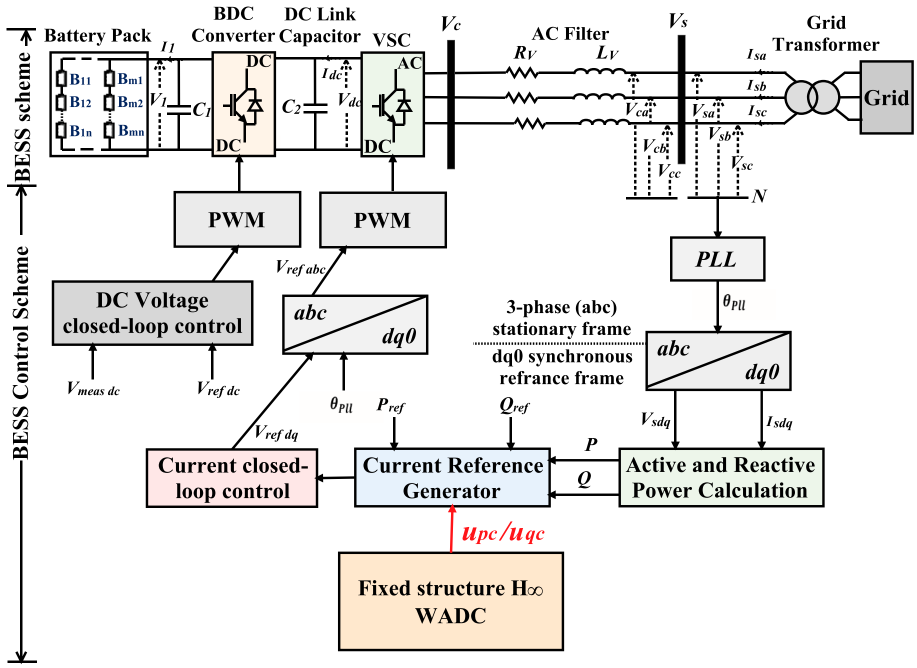

FIGURE 1 A grid-connected battery energy storage system with integrated control

$$\begin{cases} \frac{dI_L}{dt} = 0 - \frac{V_1}{L} - \frac{(1-\alpha_1)}{L} V_{dc} \\ \frac{dV_1}{dt} = -\frac{I_L}{C_1} - \frac{V_1}{C_1 R_b} + \frac{V_b}{C_1 R_b}, \\ \frac{V_{dc}}{dt} = -\frac{(1-\alpha_1)}{C_2} I_L + \frac{I_{dc}}{C_2} \end{cases} \tag{1}$$

where V_1 is the battery pack terminal voltage, I_L is the inductor current, I_{dc} is the dc-link current, V_{dc} is the dc-link voltage, V_b is the battery cell voltage, R_b is the battery's internal resistance, bidirectional converter duty cycle is denoted by α_1, and its capacitance and inductance are designated by C_1, C_2, and L, respectively.

2.1.3 | VSC model

The dynamics of the VSC, transformer, and filter reactances, respectively, that connect the VSC to the grid can be represented using the dq equations:

$$\begin{cases} L_V \frac{dI_{cd}}{dt} = \left(V_{cd} - V_{sd} - R_V I_{cd} + \omega_0 L_V I_{cq}\right) \\ L_V \frac{dI_{cq}}{dt} = \left(V_{cq} - V_{sq} - R_V I_{cq} - \omega_0 L_V I_{cd}\right) \end{cases}, \tag{2}$$

where the VSC's dq reference frame voltages are $V_{cd} = 0.5 m_d V_{dc}$ and $V_{cq} = 0.5 m_q V_{dc}$. m_d and m_q are the modulation index of VSC in dq reference frame. V_s, V_c, and I_c represent the grid voltage, VSC voltage, and current, respectively. The aggregated inductance and resistance of the VSC, transformer, and filter are L_V, R_V.

2.1.4 | Control approach for grid-integrated BESS

The commonly employed two-level control approach for grid-integrated BESS is depicted in Figure 2. The primary level control is responsible for sustaining the constant DC-link voltage (V_{dc}) and the voltage level (V_{sd}) at the coupling point. The dq-axis reference current $\left(I_{dqref}\right)$ generating for the primary-level control is given as

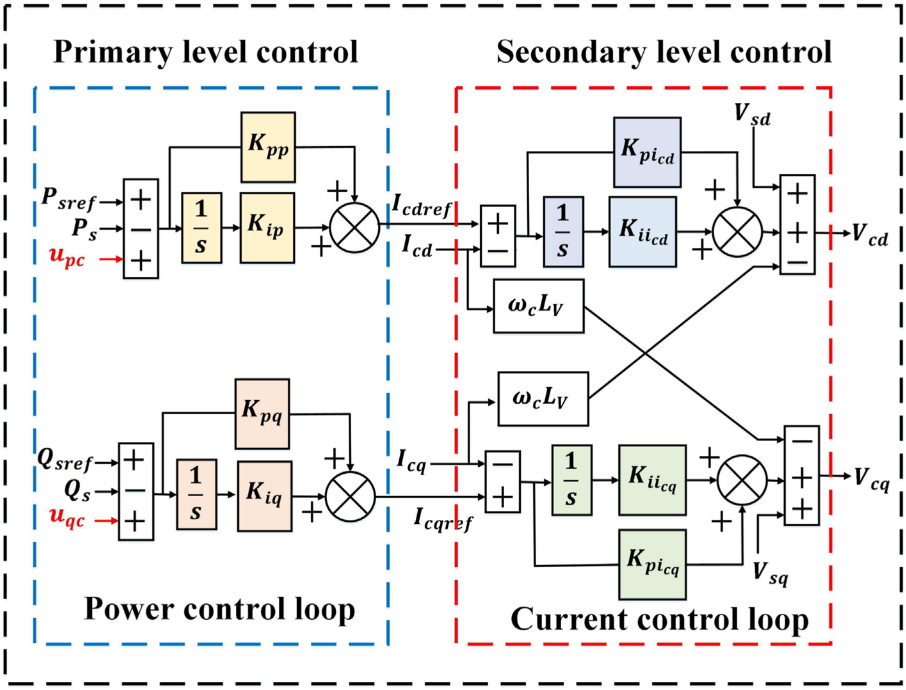

FIGURE 2 Control strategy for battery energy storage system

$$\begin{cases} I_{cdref} = (P_{sref} - P_s + u_{pc})\left(K_{pp} + \dfrac{K_{ip}}{s}\right) \\ I_{cqref} = (Q_{sref} - Q_s + u_{qc})\left(K_{pq} + \dfrac{K_{iq}}{s}\right) \end{cases}, \tag{3}$$

where u_{pc} and u_{qc} are the damping control signal of the WADC and K_{pp}, K_{pq}, K_{ip}, and K_{iq} are the PI controller gain coefficients of the primary level controller of the BESS.

The primary goal at the secondary level of the control strategy is to control power at the BESS integration point. This control is achieved by adjusting the VSC's modulation index (m_{dq}). Voltage-oriented control (VOC), which is one of the control methods, is demonstrated in Wu et al.[23] VOC operates to convert the three-phase (abc) signal stationary frame to the $dq0$-axis synchronous reference frame and vice versa. A phase-locked loop (PLL) is used to measure angle $\theta_{pll} = \tan^{-1}\left(\frac{V_{sd}}{V_{sq}}\right)$, at the point of BESS integration. So that $V_{sd} = V_s$ and $V_{sq} = 0$, direct axis voltage V_{sd} is then aligned with the grid voltage V_s to accomplish VOC. Now, the grid's active and reactive power that BESS delivers may be calculated as

$$\begin{cases} P_s = 1.5(V_{sd}I_{cd} + V_{sq}I_{cq}) = 1.5V_{sd}I_{cd} \\ Q_s = 1.5(V_{sq}I_{cd} - V_{sd}I_{cq}) = -1.5V_{sd}I_{cq} \end{cases}. \tag{4}$$

Under the lossless condition, active power received at the AC side of the VSC should be equivalent to active power delivered from the dc side of the VSC. $P_s = 1.5V_{sd}I_{cd} = V_{dc}I_{dc}$; thus, current injected by DC-to DC bidirectional converter is $I_{dc} = 1.5\left(\frac{V_{sd}I_{cd}}{V_{dc}}\right)$. The currents along the q and d axis are cross-coupled, which means that the I_{cq} depends on the I_{cd} and vice versa. Thus, as seen in Figure 2, the decoupled controller came into the picture.

2.2 | Small-signal analysis

This work aims to design a WADC for a BESS to improve the damping performance of LFO in the power system. Power flows in each transmission network are considered the system's outputs, while the BESS primary level controllers, P_{sref}

and Q_{sref}, are chosen as inputs. The entire system, including the BESS, is linearized for these inputs and outputs at the stable equilibrium point, and the state-space model of the system is described as follows:

$$\begin{cases} \frac{d\Delta X}{dt} = A\Delta X + B_i \Delta u_i \\ \Delta y_i = C_i \Delta X \end{cases}, \tag{5}$$

where the system state, output, and input vectors are $x \in \mathfrak{R}^{e \times e}$, $y_i \in \mathfrak{R}^{g \times e}$, and $u_i \in \mathfrak{R}^{e \times f}$, respectively. The system input, output, and state matrices are $B_i \in \mathfrak{R}^{e \times f}$, $C_i \in \mathfrak{R}^{g \times e}$, and $A \in \mathfrak{R}^{e \times e}$, respectively. The number of state variables is e, the number of input signals is f, and the number of output signals is g.

2.2.1 | Time delay in feedback signals

The 2nd-order Pad'e approximation is used in this study to describe time delays, and it is given as[24]

$$G_{(T_d)}(s) = \frac{-2T_d s + 6}{s^2 T_d^2 + 4T_d s + 6} = \frac{\frac{-2}{T_d s} + \frac{6}{T_d^2}}{s^2 + \frac{4}{T_d s} + \frac{6}{T_d^2}}, \tag{6}$$

where time delay is represented by T_d and the state-space model from the above transfer function can be obtained as

$$\begin{cases} \frac{d\Delta X_{T_d}}{dt} = A_{T_d} \Delta X_{T_d} + B_{T_d} \Delta u_{T_d} \\ \Delta y_{T_d} = C_{T_d} \Delta X_{T_d} \end{cases}, \tag{7}$$

where the time delay models of system input, output, and system matrices are B_{T_d}, C_{T_d}, and A_{T_d}, respectively.

The without time delay system model in (5) is cascaded with the with time delay system model in (7) to determine the complete time-delayed modal of the power system as follows:

$$\begin{cases} \frac{d\overline{\Delta X}}{dt} = \overline{A}_i \overline{\Delta X} + \overline{B}_i \Delta u_i \\ \Delta y_i = \overline{C}_i \overline{\Delta X} \end{cases}, \tag{8}$$

where $\overline{x}$ is the time-delayed system's state vector and the relevant system, input, and output matrices are given by

$$\overline{A}_i = \begin{bmatrix} A & 0 \\ B_{T_d} & A_{T_d} \end{bmatrix}, \overline{B}_i = \begin{bmatrix} B_i \\ 0 \end{bmatrix}, \overline{C}_i = [0 \quad C_{T_d}]. \tag{9}$$

3 | APPROACH FOR CHOOSING THE LOCATION, CONTROL LOOP, AND FEEDBACK SIGNAL FOR BESS

3.1 | Residue index

It is worth mentioning that residue analysis is well established in the literature to address damping controller position and feedback signal selection in the context of power system LFO study. However, the residue index is not discussed for power system operating condition variations. This paper aims to determine the best position for BESS and its damping control loop. The residue index is exploited for subsequent analysis.

The plant model's residue matrix can be derived using (5) the transfer-function representation,[25] as per the following:

$$G(s) = C(sI - A)^{-1}B = \sum_{i=1}^{e} \frac{R_i}{s - \lambda_i}, \tag{10}$$

where R_i is the residue index of $G(s)$ associated with LFO mode i, at eigenvalue λ_i, which may be further written as

$$R_i = CM_iN_i^TB, \tag{11}$$

where N_i^T and M_i are the left and the right eigenvector matrices related to the eigenvalue λ_i, respectively. Both are the ith element of the modal matrix and are associated with the state matrix stated in (5).

3.2 | BESS selection approach

In a conventional approach, the location of the BESS installation, the feedback signal, and the control loop are selected[26] as follows:

$$M_p = Max[(R_i(\rho, \gamma_0)], \tag{12}$$

where ρ is the set of each candidate's installation positions, feedback signals, and control loops; M_p is the consequence of the choice; $M_p \in \rho$; and γ_0 is the steady-state operating condition.

The residue index will vary under various operating scenarios even though the installation position, feedback signal, and control loop are all the same. Therefore, (12) isn't always the perfect approach under a changing operating scenario.

To overcome the problem of the conventional approach described in (12), an alternative approach is proposed in this work for choosing the BESS installation position, feedback signal, and control loop under the variation of system operating conditions as follows:

$$M_p = Max[min(R_i(\rho, \Phi(\gamma)))], \tag{13}$$

where $\Phi(\gamma)$ is a collection of various operating conditions, such as an increase or decrease in load and a change in network configuration. Depending on the inter-area oscillation mode of interest, there is a minimal magnitude of residue index under various operating conditions for each element of ρ. The operating condition γ_p that results in minimum residue magnitude is considered optimal operating condition. M_p (i.e., optimal BESS location, feedback signal, and control loop) is decided based on maximal of minimum residues under different values of ρ for the optimal operating condition γ_p. The selection results from M_p corresponds to least efficient damping in the ith inter-area mode at the operating condition $\gamma_p \in \Phi(\gamma)$, according to (13). As a result, if we select γ_p as the operating condition in the system to design the BESS-based damping controller, an efficient design at M_p can confirm its efficacy for all other operating conditions in $\Phi(\gamma)$. Therefore, (13) is a robust approach for choosing the BESS installation position, the feedback signals, and the control loop.

4 | DESIGN OF WADC USING FIXED STRUCTURE CONTROL SCHEME

4.1 | Framework of fixed structure control scheme

The fixed-structure controller, the standard form model, is shown in Figure 3 and consists of two primary components:

1. All non-tunable (fixed) blocks in the control system are combined in the linear time-invariant plant model $P(s)$.

2. A structured controller that combines all tunable elements of the controller is $K(s) = \text{Diag}\ (K_1(s),...,K_N(s))$. It is assumed that each control element $Kj(s)$ is linearly time-invariant and has a predetermined structure.

The system's external inputs, such as disturbances and reference signals, are collected in w, while its performance-related outputs, such as error signals, are collected in z. The linear fractional transformation yields the closed-loop transfer function from w to z, denoted $Fl(P(s),K(s))$, as follows[27]:

$$T_{zw} = Fl(P,K) = P_{zw} + P_{zu}K\left(I - P_{yu}K\right)^{-1}P_{yw}. \tag{14}$$

4.2 | Fixed-structure H_∞ controller synthesis

The fixed-structure H_∞ control scheme for BESS is shown in Figure 4. The design objective is to minimize the H_∞ norm of $Fl(P(s),K(s))$. The solution objective for optimal H_∞ problem is to identify an internally stabilizing controller $K(s)$, where $\| Fl(P(s),K(s))\|_\infty$ is reduced.[27]

PSS is considered a fixed-structure damping controller, including a controller gain, a washout filter, and a phase compensation filter. Using parametric models for such components is only reasonable, given that our strategy is optimization-based. For instance, six scalars K_c, T_{wc}, T_{1c}, T_{2c}, T_{3c}, and T_{4c} can be used to parameterize a PSS as

$$K(s) = K_c\left(\frac{sT_{wc}}{sT_{wc}+1}\right)\left(\frac{sT_{1c}+1}{sT_{2c}+1}\right)\left(\frac{sT_{3c}+1}{sT_{4c}+1}\right). \tag{15}$$

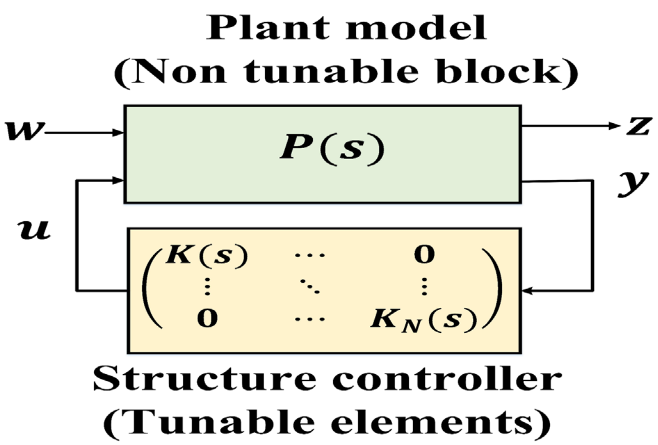

FIGURE 3 Fixed-structure controller standard form model

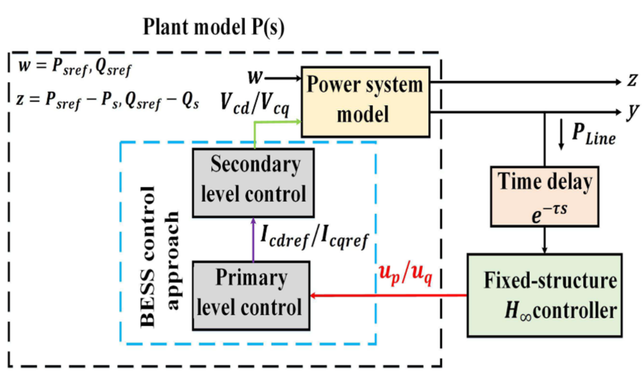

FIGURE 4 Fixed-structure H_∞ control scheme for BESS

The optimization problem of fixed-structure H_∞ controller is solved using nonsmooth optimization. The objective is to identify optimal fixed-structure controller $K(s)$ design parameters that minimize the H_∞ norm considering all internal stability constraints.[28]

$$\begin{aligned} &\underset{K(s)}{\text{minimize}} \, \| Fl(P(s),K(s)) \|_\infty \Leftrightarrow \\ &\underset{x \in \Re^k}{\text{minimize}} \, \underset{\omega[0,\infty]}{\max} \, \overline{\sigma}(Fl(P(j\omega),x)) \end{aligned}, \tag{16}$$

where the vector x collects all the tunable parameters in fixed-structure controller $K(s)$. The nonsmooth optimization-based control problem is solved using MATLAB-based *hinfstruct* function.

4.3 | Procedure to design fixed-structure WADC

1. Linearize the entire power system at robust operating condition γ_p.
2. Small-signal analysis is used to identify the system's inter-area oscillation modes, and the dominant inter-area oscillation modes are then determined based on frequency and damping ratio.
3. Use residue analysis to identify the appropriate feedback signal with a time delay for the dominant inter-area oscillation mode.
4. The full-order power system is converted to a reduced-order system model using the Schur model reduction method[29] to design WADC for BESS.
5. The reduced-order system is converted into the standard model form, which has a non-tunable block (plant model), and tunable sections (structured controller), in the fixed-structure control design problem.
6. In this study, PSS is regarded as a fixed-structure, and parametric models are used to characterize the structure of each tunable element of fixed-structure controller $K(s)$.
7. The fixed-structure controller $K(s)$ design parameters minimize the H_∞ norm $\| Fl(P(s),K(s)) \|_\infty < 1$ while adhering to internal stability constraints.
8. The fixed-structure controller $K(s)$ parameters are tuned using the *hinfstruct* function in MATLAB.
9. Validate the proposed WADC system's performance in various operating scenarios.

4.4 | Flowchart of the proposed scheme

The flowchart in Figure 5 shows the proposed scheme and usage details to be presented in the subsequent sections.

5 | VALIDATION ON MODIFIED NEW ENGLAND 10-MACHINE BENCHMARK SYSTEM

5.1 | Study system description and small signal analysis

The modified IEEE-39 bus benchmark power system is depicted in Figure 6. This test system consists of 10 SGs, 39 buses, 46 transmission lines, 21 loads, 12 transformers, and six inter-area tie lines, with a total generation capacity of 6,248.9 MW. The system base is set at 100 MVA and 60 Hz, with the power ratings of each generator being different, as discussed in Hiskens.[30] The primary and secondary voltage ratings of each transformer connecting the generator buses in the IEEE 39-bus system are 11.3 and 345 kV, respectively. Additionally, each bus connected to the transmission lines operates at a voltage rating of 345 kV. This test system is divided into three areas: SG1–SG3 are in Area 1, SG4–SG7 are in Area 2, and SG8–SG10 are in Area 3. Moreover, every excitation system of SGs equipped with local PSS, excluding SGs G1, G5, G7, and G8, has a gain that is 25 times greater than the PSS data obtained from Hiskens.[30]

In this work, we differentiate between two configurations in a multi-machine power system: one without BESS, termed the base case (BC), and the other incorporating BESS, known as Case 1 (CS1). The main objective is to assess the system's damping ability to mitigate inter-area oscillations across various operating conditions. Table 1 provides a

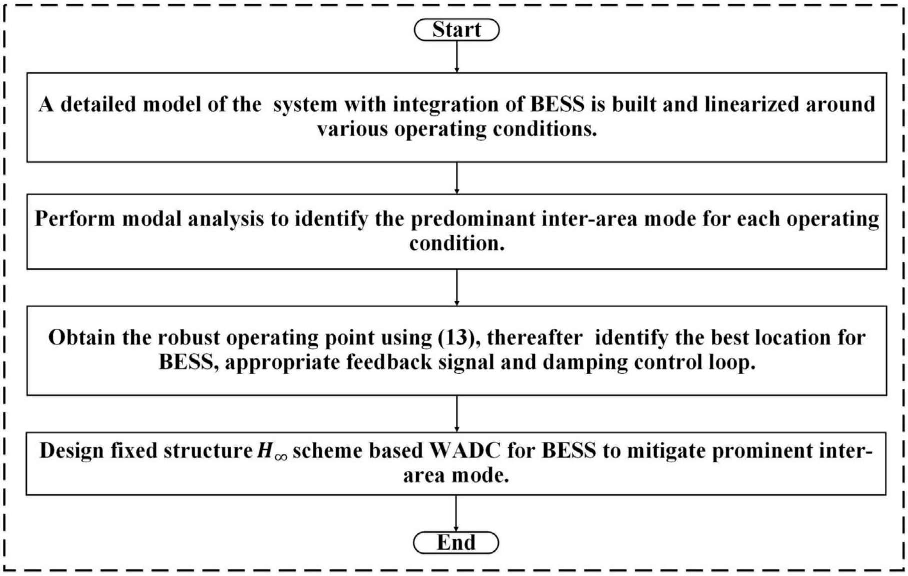

FIGURE 5 Flowchart of the proposed scheme

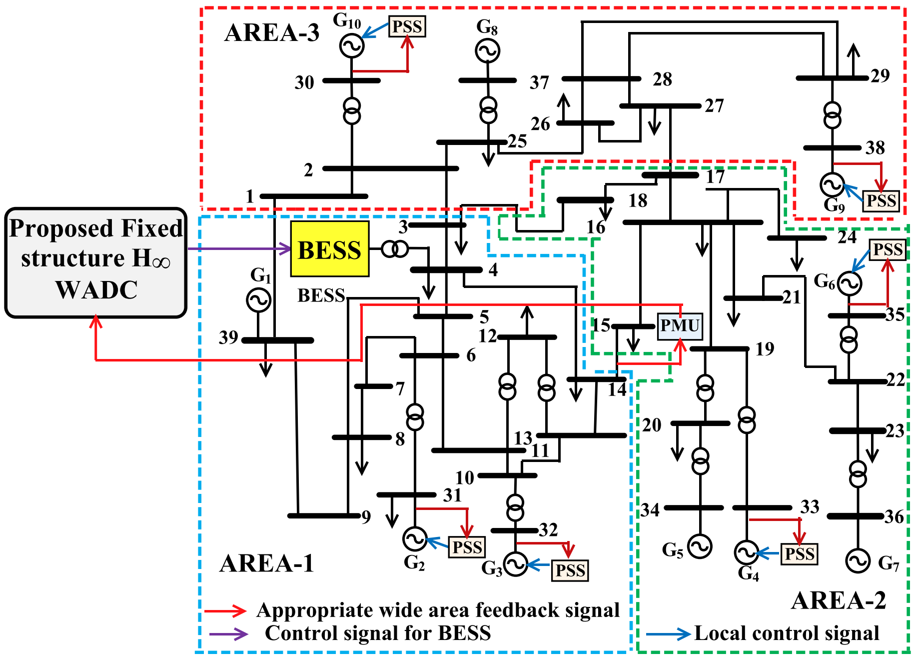

FIGURE 6 Single-line diagram of the IEEE 39 bus system integrated with BESS

comprehensive overview of the various operational conditions explored in this study, identified as γ_{p1}, γ_{p2}, γ_{p3}, and γ_{p4}, respectively. The small-signal analysis is conducted for the base case configuration of the study test system to examine the prominent inter-area oscillation mode under different operational scenarios. The results are summarized in Table 2, focusing primarily on the dominant inter-area oscillation mode, while other LFO modes are not listed.

Furthermore, the SGs in Area 3 actively participate in the dominant inter-area oscillation mode in the base case under different operating conditions, as shown in Figure 7. So, at Bus 27 (Area 3), a 50 MW BESS rating is incorporated with the study test system to provide power requirements under any additional loading scenario. The parameters of BESS are taken from Calero et al.[19] In this simulation analysis, BESS operates in discharging mode, with the initial state of charge (SOC) of BESS being taken as 80%. Under normal operating conditions, a BESS is integrated on Bus 27, and this system has an inter-area mode present as (). Furthermore, for Case 1, Table 2 comprehensively presents the dominant inter-area oscillation mode and the residue index of the system across various operating conditions, providing valuable insights into the system's dynamic behavior.

In Table 2, in the base case, we observe that the damping ratio of mode M1 is obtained as 4.70%, which is increased to 5.61% in case1 under γ_{p1} operating condition. However, in operating condition γ_{p2}, the damping ratio of mode M2 is obtained as 6.26%, which is reduced to 5.96% in Case 1. The damping ratios of Modes M3 and M4 are obtained as 6.54% and 6.46% in base case under operating conditions γ_{p3} and γ_{p4}; these ratios again increased to 6.87% and 6.45% in Case 1. So it can be observed that the damping performance in Case 1 exhibits a marginal improvement when compared to the base case for the dominant inter-area mode across different operating conditions.

As shown in Table 2, the minimal magnitude of the residue index (0.0018) is obtained under the operating condition γ_{p4}. Therefore, in this research, operating condition γ_{p4} is chosen for designing the WADC for the BESS.

5.2 | Frequency response of study system

The frequency response (Bode plot) of the study system under steady-state condition, both without and with BESS, is shown in Figure 8A,B, respectively. In the system without BESS, a gain margin of 32.4 dB is observed at a phase crossover frequency of 16.1 rad/s, along with a phase margin of 49° at a gain crossover frequency of 0.892 rad/s. Conversely, the system with BESS exhibits a gain margin of 45.6 dB at a phase crossover frequency of 20.4 rad/s and a phase margin

TABLE 1 Power system operating conditions

$\Phi(\gamma_p)$	System operating conditions description
γ_{p1}	Active and reactive power of loads at Area 1 (Buses 31 &39) increases by 10%
γ_{p2}	Active and reactive power of loads at Area 2 (Buses 20 & 23) increases by 10%
γ_{p3}	Active and reactive power of loads at Area 3 (Buses 25 & 29) decreases by 10%
γ_{p4}	The permanent outage of the inter-area line between Buses 2 & 3

TABLE 2 Damping ratio of the study system in the base case and case1 for different operating conditions

$\Phi(\gamma_p)$	Mode	Damping ratio in base case	Damping ratio in Case 1	Residue index of Case 1
γ_{p1}	M1	$-0.252 \pm i5.366$ ($\xi = 4.70\%, f = 0.85$ Hz)	$-0.230 \pm i4.095$($\xi = 5.61\%, f = 0.65$ Hz)	$0.0189\angle \mp 13.34^\circ$
γ_{p2}	M2	$-0.339 \pm i5.408$($\xi = 6.26\%, f = 0.86$ Hz)	$-0.305 \pm i5.116$($\xi = 5.96\%, f = 0.81$ Hz)	$0.0042\angle \pm 103.72^\circ$
γ_{p3}	M3	$-0.352 \pm i5.376$($\xi = 6.54\%, f = 0.85$ Hz)	$-0.269 \pm i3.910$($\xi = 6.87\%, f = 0.62$ Hz)	$0.0210\angle \pm 146.35^\circ$
γ_{p4}	M4	$-0.353 \pm i5.452$($\xi = 6.46\%, f = 0.86$ Hz)	$-0.33 \pm i5.154$($\xi = 6.45\%, f = 0.82$ Hz)	$0.0018\angle \mp 48.16^\circ$

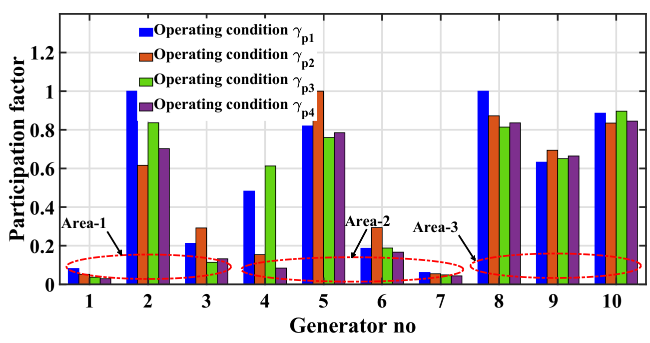

FIGURE 7 Participation factor of synchronous generators in the dominant oscillation mode in the base case under various operating conditions

of 107.5° at a gain crossover frequency of 0.796 rad/s. These results indicate that incorporating BESS increases both the gain and phase margins of the system. Consequently, the damping performance and overall stability of the system are enhanced compared to the system without BESS.

5.3 | Choice of BESS installation position, feedback signal, and damping control loop

The candidate group $\Omega(\rho)$ is chosen in this work, as shown in Table 3, for analyzing the impact of grid-connected BESS in system inter-area oscillation mode under the variation of power system operating conditions.

Under the operating condition γ_{p4}, the residue index magnitude of the system is depicted in Figure 9. From Figure 9, the maximal magnitude of the residue index is 0.0795 at candidate group ρ_9 (i.e., reactive power control loop). The candidate group ρ_9 is the best choice by the conventional approach according to (12); in this case, the BESS installation position at Bus 4 (Area 1), the feedback signal is the power flow over an inter-area tie line P_{15-14} (between Areas 2 and 3), and the damping control loop is the reactive loop of BESS.

From Figure 9, the maximal of all the minimal magnitude of residue index is 0.0054 at candidate group ρ_4 (i.e., active power control loop). The candidate group ρ_4 is the best choice by the robust approach according to (13); in

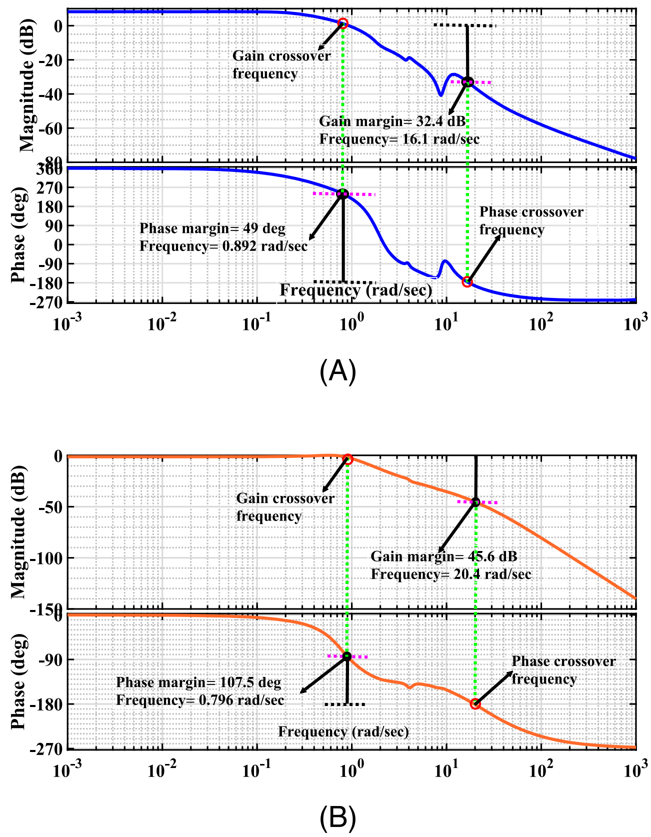

FIGURE 8 Bode plot of the study system: (A) without BESS and (B) with BESS

TABLE 3 Candidate group of study system

Candidate group $\Omega(\rho)$	Collection of candidate groups
Candidate BESS location	Bus 4 (Area 1), Bus 22 (Area 2), & Bus 27 (Area 3)
Candidate damping control loops	Active & reactive power control loops
Candidate feedback signals of the damping controller	Power flow through lines P_{26-27}, P_{27-17} (between Areas 3 and 2), P_{1-39} (between Areas 3 and 1), P_{15-14} (between Areas 2 and 1), & rotor speed deviation $\Delta\omega_{4-8}$ (Areas 2 to 3)

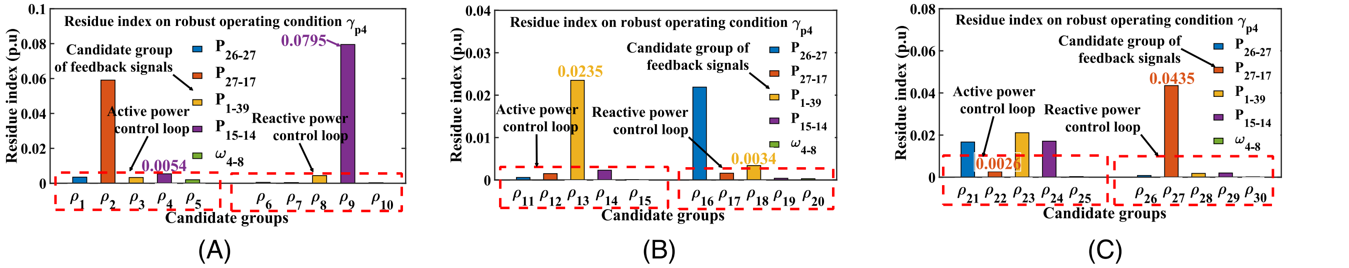

FIGURE 9 Residue index of study system under operating condition γ_{p4}. (A) BESS installed on Bus 4, (B) BESS installed on Bus 22, and (C) BESS installed on Bus 27

this case, the BESS installation position is at Bus 4, the feedback signal is the power flow over an inter-area tie line P_{15-14}, and the active power loop of BESS is the damping control loop.

According to Figure 9A–C, we draw conclusions about this analysis.

1. The robust choice between each candidate in $\Omega(\rho)$ is the candidate group ρ_4. The minimal magnitude of the residue index of the candidate group ρ_4 is the maximal in each lower residue index magnitude of candidates in $\Omega(\rho)$. Thus, candidate group ρ_4 is the best choice found based on (13), which states that the BESS should be placed at Bus 4; the feedback signal is the power flow over an inter-area tie line P_{15-14}; and the active power loop of BESS is the damping control loop.
2. BESS installation on Bus 4 is superior to Buses 22 and 27.
3. The feedback signal P_{15-14} is superior compared to the feedback signals P_{26-27}, P_{27-17}, P_{1-39}, and ω_{4-8}.

5.4 | Design of BESS-based WADC

The first stage in designing the proposed WADC for BESS is selecting the damping controller location and the appropriate feedback signal to improve the system's damping performance under various operating conditions. The damping control loop and feedback signal are selected using the robust selection approach outlined in Section 3.2. From Figure 9, it is determined that the active power control loop of the BESS is the optimal location to position the WADC. Furthermore, the power flow through the inter-area line P_{15-14} is the appropriate feedback signal for designing the WADC for the BESS. It is considered that the PMU is deployed on Bus 15 of the test system to get the WADC feedback signal, and the PMU utilizes IEEE C37.118.2 protocol for real-time data streaming. PMUs capture voltage, current, and frequency at high sampling rates (240 samples per second) to monitor the dynamic behavior of the IEEE 39 practical system.

In this research, we have also accounted for the communication delays in the feedback signal, i.e., minimum and maximum time delays of 100 and 150 ms, respectively. With P_{15-14} as the output of the plant model and P_{sref} as the input for the operating condition γ_{p4} with a 100 ms time delay in feedback signals, the order of the system is found to be 139. This higher order system is further reduced to a 12th-order system using the Schur model reduction approach[29] for case CS1 to reduce the WADC design's complexity. The frequency response of the 12th-order reduced system is approximately the same as the full-order system in the frequency range of (0.1–2) Hz, as shown in Figure 10. The reduced order system contains the significant inter-area oscillation mode M4 under the operating condition γ_{p4}.

5.4.1 | Design of fixed-structure H_∞ scheme-based WADC for BESS

The design procedure for the fixed-structure H_∞ scheme-based WADC is provided in Section 4.3. This study designs the proposed WADC for the BESS under the operating condition γ_{p4} in the candidate group ρ_4, where the WADC is linked to the active power control loop of the BESS. The objective is to increase the damping ratio of the relevant inter-area oscillation modes, M1 to M4, of the study system in case CS1. The *hinfstruct* function in MATLAB is used to tune the

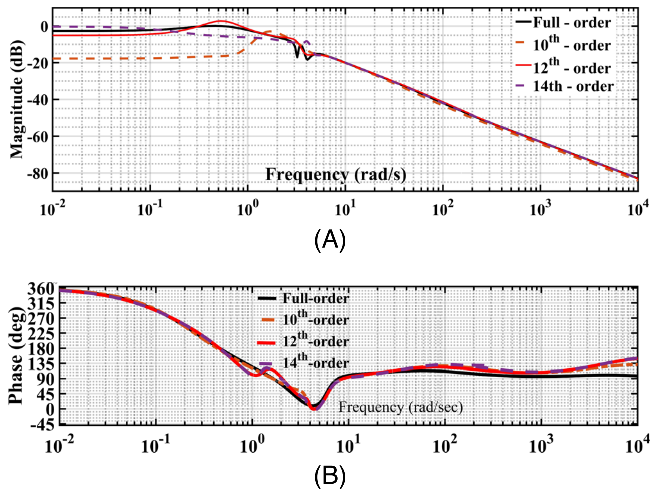

FIGURE 10 Frequency responses of the modified IEEE 39 bus system of full-order and reduced-order system under operating condition γ_{p4}

parameter of the fixed-structure damping controller (i.e., PSS). After almost 31 iterations, the H_∞ program based on nonsmooth structure optimization converges to its optimum closed-loop gain value of 1.31, which means that the H_∞ norm is almost satisfied. The damping controller's tuned parameters are $K_c = 0.851$, $T_{wc} = 10$, $T_{1c} = 0.654$, $T_{2c} = 0.0134$, $T_{3c} = 0.567$, and $T_{4c} = 0.0135$, respectively.

Moreover, in this study, the fixed-structure H_∞ WADC designed for the BESS under the operating condition γ_{p4} in the candidate group ρ_9 (i.e., WADC is linked to the reactive power control loop of BESS) is compared with the proposed WADC in the candidate group ρ_4. The H_∞ norm is not satisfied since the nonsmooth structural optimization-based H_∞ program does not converge to a solution. The best closed-loop gain value of 2.31 after around 47 iterations with parameters of the damping controller is obtained to be $K_c = 1.738, T_{wc} = 10, T_{1c} = 0.451, T_{2c} = 0.0252, T_{3c} = 0.456$, and $T_{4c} = 0.0247$, respectively.

5.4.2 | Performance evaluation of WADC

The proposed fixed-structure H_∞ scheme-based WADC's damping performance for the BESS is evaluated through modal analysis on the modified IEEE 39 bus system. The main objective is to evaluate the damping performance of the system in inter-area modes under various operating conditions. The damping performance of the dominant inter-area oscillation modes of the system wherein the WADC is associated with the candidate groups ρ_4 and ρ_9 of BESS are, respectively, shown in Tables 4 and 5. The BESS-based wide-area power system stabilizer (WAPSS) is a single-input, single-output (SISO) structure that utilizes P_{15-14} as a feedback signal. This stabilizer is connected to the secondary control loop of the BESS and is referred to as the BESS-based WAPSS throughout the study. This WAPSS scheme is implemented on the candidate groups ρ_4 and ρ_9 of BESS to evaluate the damping performance in the practical study system inter-area oscillation modes under the operating condition γ_{p4}.

The 10% damping ratio is the threshold value to assess the proposed controller's effectiveness in the study system inter-area modes under different operating conditions. The damping ratio in the inter-area mode M4 with the 100 ms time delay in the feedback signal in BESS-based WAPSS[25] in candidate group ρ_4 is less than 10%, as depicted in Table 4. The damping of the concerned inter-area oscillation modes M1 to M4 is improved beyond 10% by the proposed fixed-structure H_∞ WADC. When the proposed WADC is installed on the candidate group ρ_9, the damping ratio of concerned inter-area oscillation modes M1 to M3 is higher than 10%, except the single case of the inter-area oscillation Mode M4 with 150 ms time delay in feedback signal, where the damping ratio is slightly lower than 10%. The BESS-based WAPSS[25] is installed on the candidate group ρ_9; the damping ratio of concerned inter-area oscillation modes M1 to M4 is lower than 10% (see Table 5).

In the presence of operating condition contingencies and uncertainty associated with communication time delays in the feedback signal, the proposed fixed-structure H_∞ scheme-based WADC functions robustly for the designed

TABLE 4 Eigenvalue of system inter-area oscillation modes with WADCs in the candidate group ρ_4 of BESS

$\Phi(\gamma_p)$	Mode	T_d(ms)	BESS-based WAPSS	Proposed fixed structure WADC
γ_{p1}	M1	100	$-0.441 \pm i3.677$ ($\xi = 11.93\%$)	$-0.553 \pm i3.654$($\xi = 14.98\%$)
		150	$-0.415 \pm i4.069$ ($\xi = 10.16\%$)	$-0.527 \pm i3.749$ ($\xi = 13.92\%$)
γ_{p2}	M2	100	$-0.443 \pm i3.993$ ($\xi = 11.03\%$)	$-0.560 \pm i3.739$ ($\xi = 14.81\%$)
		150	$-0.455 \pm i4.063$ ($\xi = 11.14\%$)	$-0.538 \pm i3.707$ ($\xi = 14.38\%$)
γ_{p3}	M3	100	$-0.465 \pm i3.667$ ($\xi = 12.59\%$)	$-0.537 \pm i3.789$ ($\xi = 14.05\%$)
		150	$-0.448 \pm i3.978$ ($\xi = 11.19\%$)	$-0.556 \pm i3.715$ ($\xi = 14.80\%$)
γ_{p4}	M4	100	$-0.371 \pm i3.751$ ($\xi = 9.85\%$)	$-0.511 \pm i3.617$ ($\xi = 14.01\%$)
		150	$-0.530 \pm i5.081$ ($\xi = 10.37\%$)	$-0.527 \pm i3.749$ ($\xi = 13.92\%$)

TABLE 5 Eigenvalue of system inter-area oscillation modes with WADCs in the candidate group ρ_9 of BESS

$\Phi(\gamma_p)$	Mode	T_d(ms)	BESS-based WAPSS	Proposed fixed structure WADC
γ_{p1}	M1	100	$-0.476 \pm i4.936$ ($\xi = 9.61\%$)	$-0.420 \pm i4.039$ ($\xi = 10.36\%$)
		150	$-0.469 \pm i4.956$ ($\xi = 9.425\%$)	$-0.371 \pm i3.528$ ($\xi = 10.46\%$)
γ_{p2}	M2	100	$-0.346 \pm i4.147$ ($\xi = 8.33\%$)	$-0.450 \pm i3.854$ ($\xi = 11.6\%$)
		150	$-0.443 \pm i4.960$ ($\xi = 8.71\%$)	$-0.439 \pm i3.685$ ($\xi = 11.84\%$)
γ_{p3}	M3	100	$-0.368 \pm i4.027$ ($\xi = 9.10\%$)	$-0.384 \pm i3.619$ ($\xi = 10.55\%$)
		150	$-0.359 \pm i3.838$ ($\xi = 9.32\%$)	$-0.373 \pm i3.469$ ($\xi = 10.71\%$)
γ_{p4}	M4	100	$-0.406 \pm i4.939$ ($\xi = 8.19\%$)	$-0.400 \pm i3.942$ ($\xi = 10.19\%$)
		150	$-0.420 \pm i4.946$ ($\xi = 8.47\%$)	$-0.359 \pm i3.838$ ($\xi = 9.32\%$)

parameters. When time delay constraints are taken into consideration, the proposed WADC for BESS is capable of maintaining at least a 10% damping ratio in prominent inter-area oscillation modes. In contrast, the BESS-based WAPSS[25] is incapable of providing enough damping for critical inter-area oscillation modes.

5.5 | Computational burden of study system

This study uses MATLAB 2020a software to solve the linear analysis of the IEEE 39 bus system and design a fixed-structure H_∞ control scheme-based WADC for BESS. This analysis is carried out on a personal computer, an Intel(R) Core (TM) i7-8700 CPU @ 3.20GHz with 8 GB of installed RAM 64-bit operating system. Several factors contribute to the computational burden in terms of time to solve the proposed WADC for BESS to mitigate system inter-area oscillations, including system complexity, control structure complexity, and the complexity of H_∞ control optimization problem. The computation times are as follows: 160.406 s for the IEEE 39 bus system with PSS, 196.234 s for the IEEE 39 bus system with BESS, 424.625 s for the IEEE 39 bus system with BESS associated with WAPSS,[25] and 402.578 s for the IEEE 39 bus system with BESS combined with proposed WADC. It is observed from results that proposed approach requires less computational burden compared to WAPSS proposed in Qi et al.[25]

6 | VALIDATION OF DYNAMIC SIMULATION ON THE REAL-TIME DIGITAL SIMULATOR

The dynamic simulation of the modified IEEE 39 bus system with proposed fixed-structure H_∞ WADC for BESS is carried out on RTDS using the graphical user interface of RSCAD FX 1.3. The Real-Time Digital Simulation framework is depicted in Figure 11.

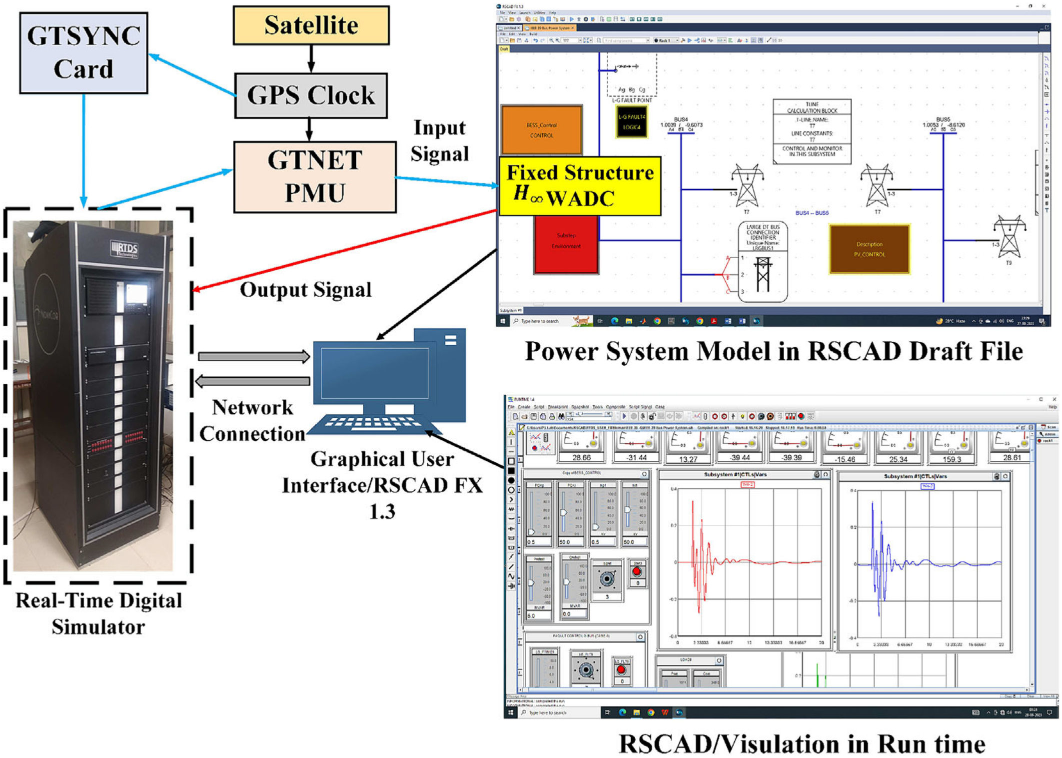

FIGURE 11 Framework for real-time simulation

The dynamic simulation of the studied test system is carried out to verify the efficacy of the proposed WADC for BESS and evaluate its performance in different operating scenarios. The different scenarios are simulated under following contingency cases:

- Scenario 1 (S1): a three-phase fault is applied at Bus 20 in Area 2 at $t = 3$ s for 100 ms.
- Scenario 2 (S2): a double line to fault is applied at $t = 3$ s for 100 ms on the transmission line between Buses 29 and 37 and considering the permanent outage on the transmission line between Buses 27 and 17 as well as Buses 3 and 4.
- Scenario 3 (S3): considering the variable communication time delay in the WADC feedback signal P_{15-14}, a line-to-ground fault is applied to the transmission line between Buses 16 and 19 at $t = 3$ s for 100 ms.
- Scenario 4 (S4): the integration of the solar photovoltaic system on Bus 20 and the three-phase fault is applied at Bus 38 at $t = 3$ s for 100 ms.

Except for Scenario S3, the simulation case for each scenario considers 100 ms communication time delay in the proposed WADC's feedback signal P_{15-14} into account.

6.1 | Scenario 1 (S1)

In this scenario, we evaluated the damping performance of proposed WADC for BESS in candidate groups ρ_4 (i.e., active control loop) and ρ_9 (i.e., reactive control loop) by conducting simulations under various operating conditions (see Table 1, γ_{p1} to γ_{p4}) of the practical study system. In this simulation scenario, the three-phase fault is applied at Bus 20 in Area 2 at 3 s with a fault duration of 100 ms to generate dynamic oscillations in the system.

The dynamic simulation response of the rotor speed deviation between SGs 4 and 2 and the DC link voltage (V_{dc}) of the BESS with the proposed WADC for BESS as well as for the WAPSS[25] in candidate group ρ_4 under different operating conditions are depicted in Figure 12. This simulation response reveals that the SG rotor oscillation and BESS DC link voltage oscillation are better damped after the occurrence of a fault, reducing peak overshoot and settling time of the rotor oscillation and DC link voltage oscillation, compared to the BESS-based WAPSS.[25] In each operating condition (γ_{p1} to γ_{p4}), the settling time of the SG rotor oscillation and DC link voltage oscillation of BESS is less than 8 s by the

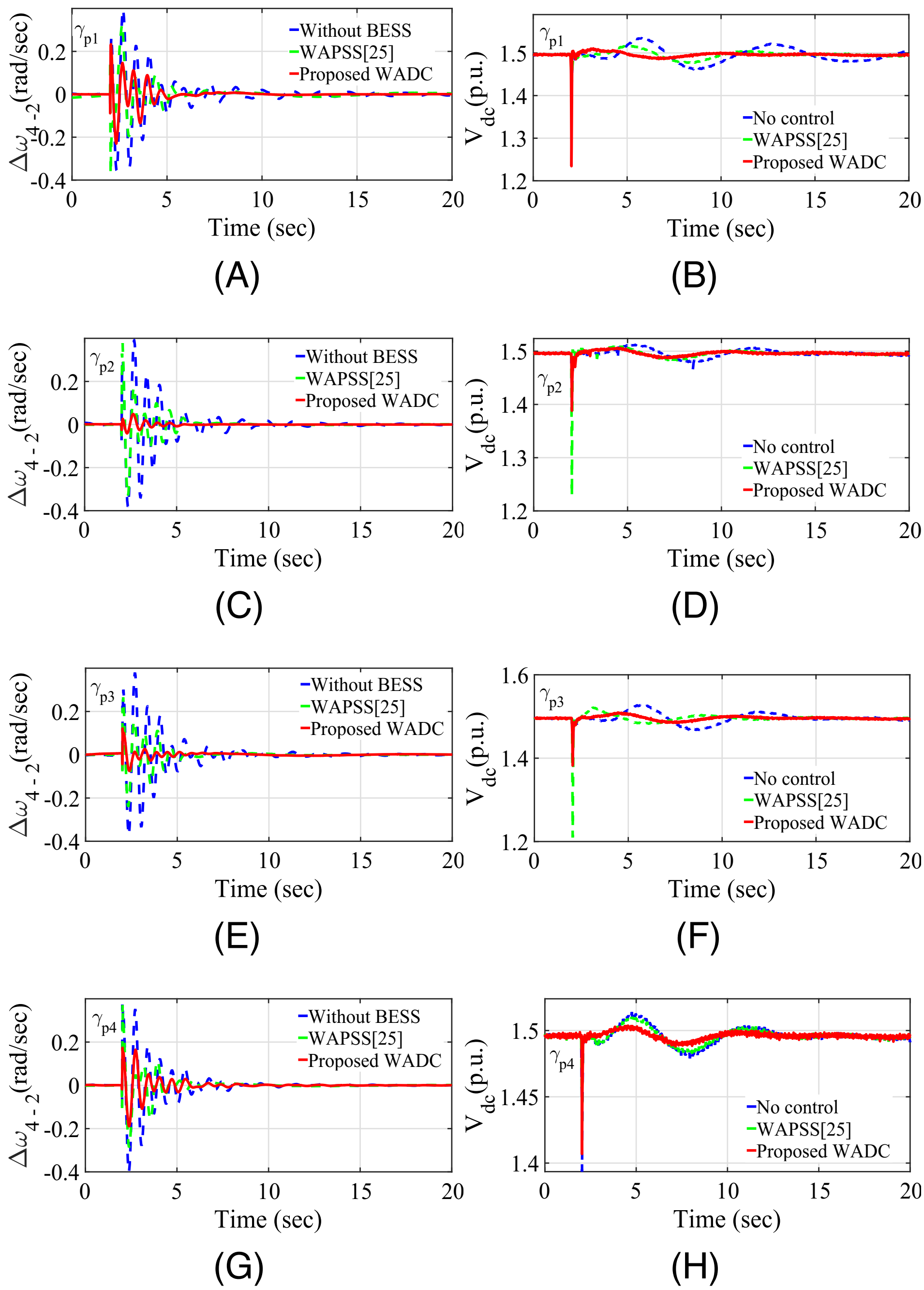

FIGURE 12 Dynamic response of the study system with a WADC for BESS in candidate group ρ_4 under various operating conditions: (A) $\Delta\omega_{4-2}$ under γ_{p1}, (B) V_{dc} under γ_{p1}, (C) $\Delta\omega_{4-2}$ under γ_{p2}, (D) V_{dc} under γ_{p2}, (E) $\Delta\omega_{4-2}$ under γ_{p3}, (F) V_{dc} under γ_{p3}, (G) $\Delta\omega_{4-2}$ under γ_{p4}, and (H) V_{dc} under γ_{p4}

proposed WADC. Further, the peak overshoot of both the SG rotor oscillation and the DC link voltage of the BESS effectively reduced, as shown in Figure 12.

Additionally, Figure 13 illustrates the dynamic response of the proposed WADC as well as of WAPSS[25] for BESS in candidate group ρ_9. This simulation response includes the rotor speed deviation between SGs 4 and 2 and the DC link voltage of the BESS under various operating conditions. The proposed WADC for BESS demonstrates superior damping performance compared to the BESS-based WAPSS.[25] However, in candidate group ρ_9, the rotor oscillation and BESS DC link voltage oscillation settling time are slightly increased compared to candidate group ρ_4. Unlike the WADC for BESS in candidate group ρ_9, the proposed WADC for BESS in candidate group ρ_4 effectively damps the prominent inter-area oscillations of the study system under various operating conditions.

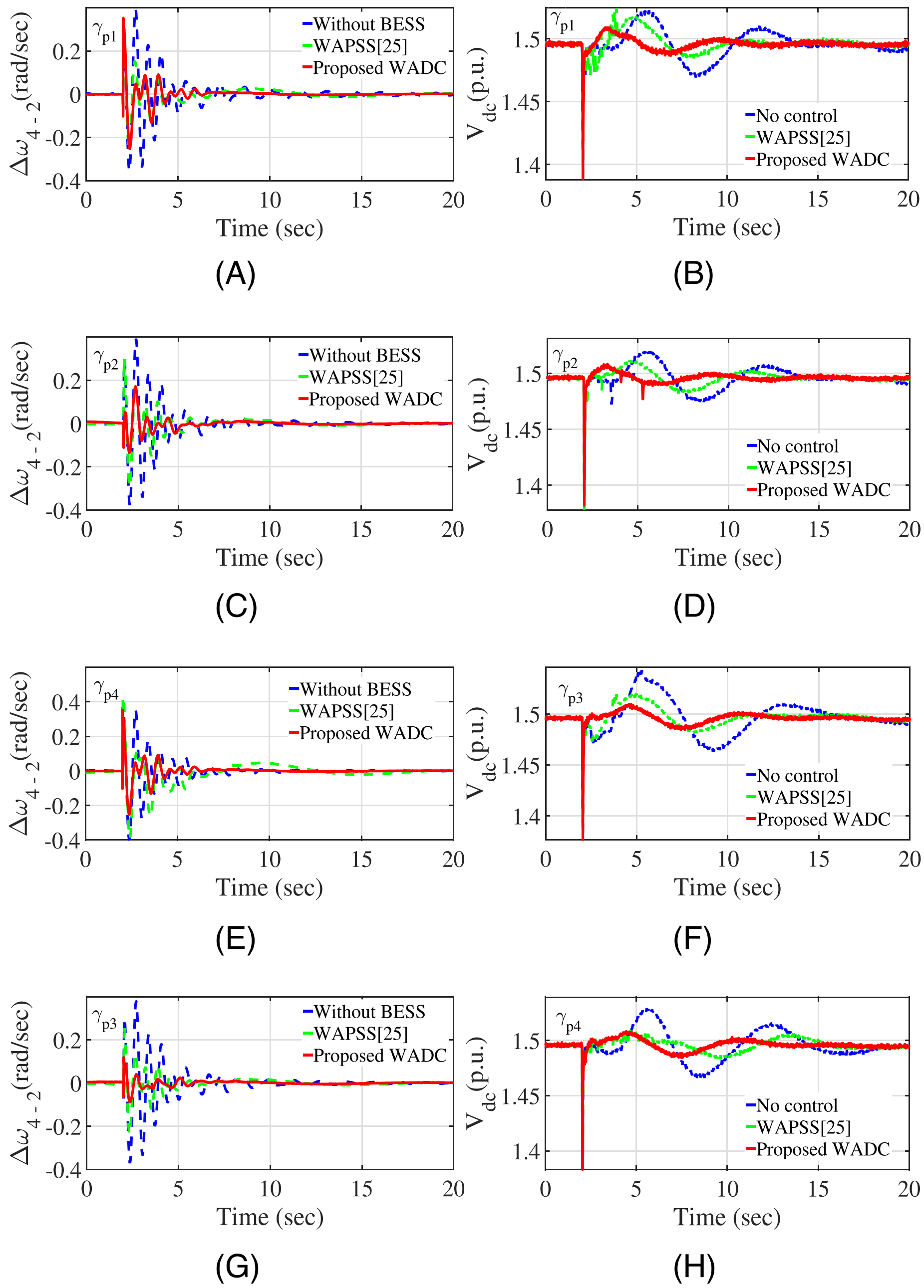

FIGURE 13 Dynamic response of the study system with a WADC for BESS in candidate group ρ_9 under various operating conditions: (A) $\Delta\omega_{4-2}$ under γ_{p1}, (B) V_{dc} under γ_{p1}, (C) $\Delta\omega_{4-2}$ under γ_{p2}, (D) V_{dc} under γ_{p2}, (E) $\Delta\omega_{4-2}$ under γ_{p3}, (F) V_{dc} under γ_{p3}, (G) $\Delta\omega_{4-2}$ under γ_{p4}, and (H) V_{dc} under γ_{p4}

6.2 | Scenario 2 (S2)

In this scenario, the practical study system is simulated with a double line fault applied at $t = 3$ s for a duration of 100 ms on the transmission line between Buses 29 and 37. The simulation aims to assess the damping performance of the proposed WADC, which is linked to candidate groups ρ_4 and ρ_9 of the BESS under operating condition γ_{p1}. The dynamic simulation responses, including the rotor speed deviation between SGs 4 and 2, the power flow through line (P_{4-14}), the BESS active power, and the DC link voltage of the BESS, are depicted in Figure 14.

From this simulation response, it is revealed that the proposed WADC provided adequate damping to mitigate the SG rotor oscillation, power oscillation in the transmission line, BESS active power oscillation, and BESS DC link voltage oscillation, performing more effectively compared to the BESS-based WAPSS.[25] The settling time of the rotor oscillation, power oscillation in the transmission line, BESS active power oscillation, and the DC link voltage oscillation of

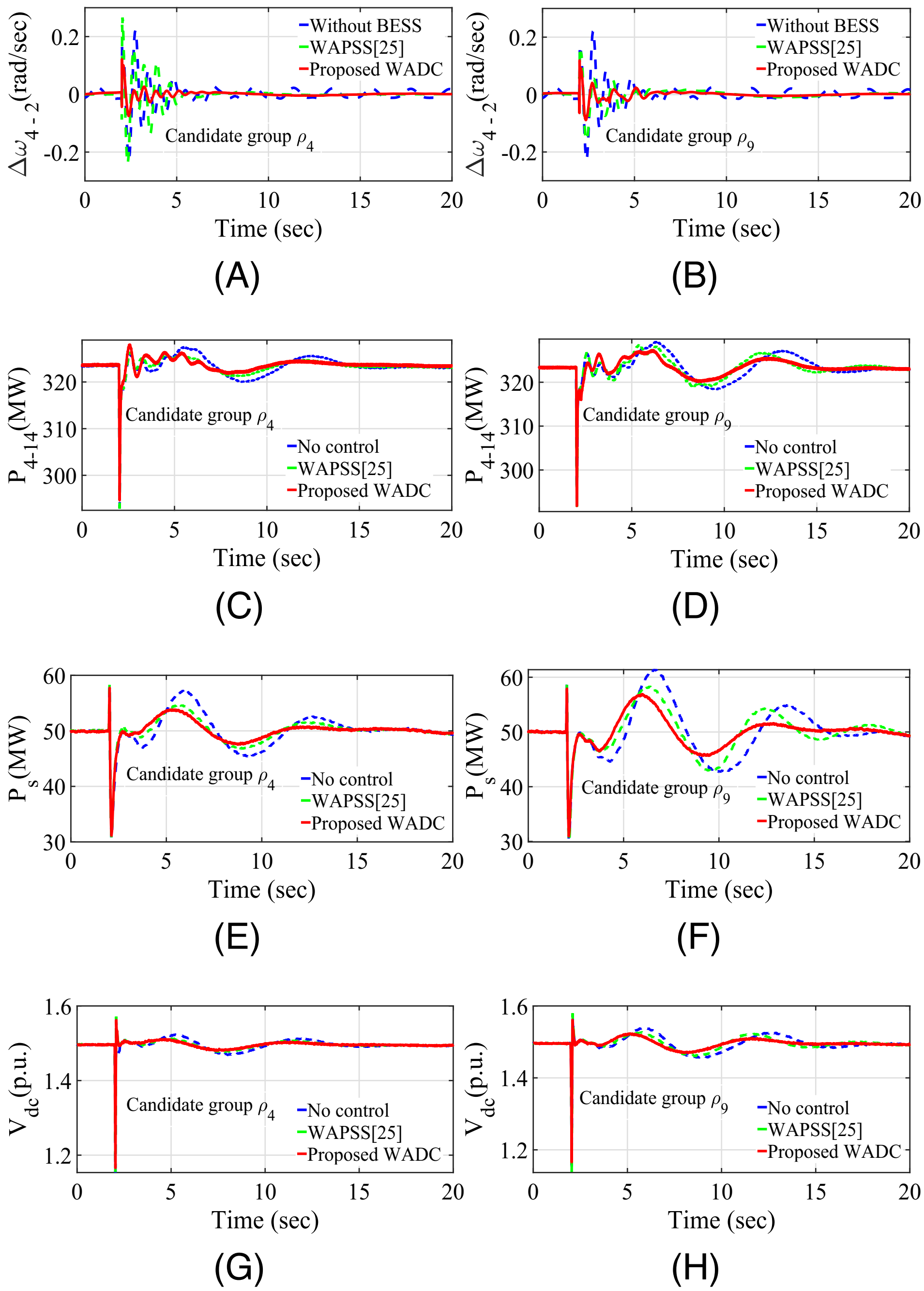

FIGURE 14 Dynamic response of the study system with a WADC for BESS in candidate groups ρ_4 and ρ_9 under operating condition γ_{p1}: (A) $\Delta\omega_{4-2}$ under ρ_4, (B) $\Delta\omega_{4-2}$ under ρ_9, (C) P_{4-14} under ρ_4, (D) P_{4-14} under ρ_9, (E) P_s under ρ_4, (F) P_s under ρ_9, (G) V_{dc} under ρ_4, and (H) V_{dc} under ρ_9

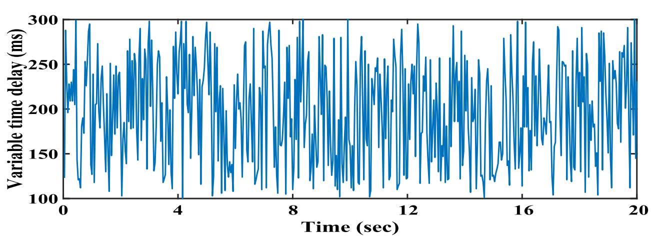

FIGURE 15 Variable communication time delays

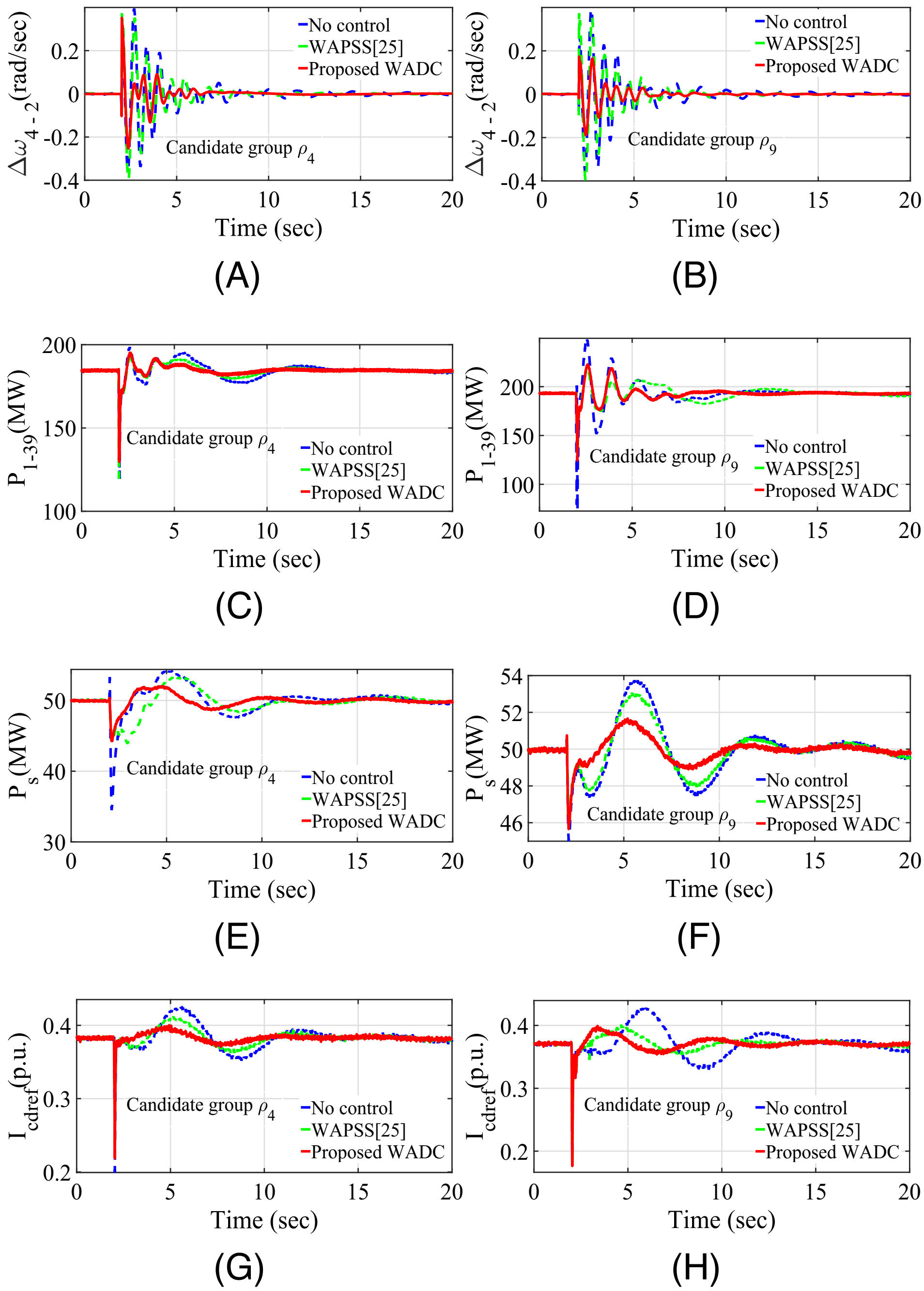

FIGURE 16 Dynamic response of the study system with a WADC for BESS in candidate groups ρ_4 and ρ_9 under operating condition γ_{p1}: (A) $\Delta\omega_{4-2}$ under ρ_4, (B) $\Delta\omega_{4-2}$ under ρ_9, (C) P_{1-39} under ρ_4, (D) P_{1-39} under ρ_9 (E) P_s under ρ_4, (F) P_s under ρ_9, (G) I_{cdref} under ρ_4, and (H) I_{cdref} under ρ_9

BESS in scenario S2 is slightly increased compared to the dynamic simulation response in Scenario S1 under operating condition γ_{p1}. The damping performance of the WADC linked with candidate group ρ_4 is better than that with candidate group ρ_9 of the BESS, as shown in Figure 14.

6.3 | Scenario 3 (S3)

This simulation scenario assesses the robustness of the controller's performance against the variable communication time delay uncertainty in the feedback signal P_{15-14} of the proposed WADC, as shown in Figure 15. This analysis employed variable communication delay range from 100 to 300 ms. The practical study system, incorporating the proposed WADC linked with BESS candidate groups ρ_4 and ρ_9, is simulated under operating condition γ_{p1}. During this simulation, a line-to-ground fault is applied to the transmission line connecting Buses 16 and 19, lasting for 100 ms starting at $t = 3$ s. The dynamic simulation response encompasses the rotor speed deviation between SG 4 and 2, the power flow through the inter-area line (P_{1-39}), BESS active power, and the d-axis reference current of the VSC for BESS, as depicted in Figure 16.

The results depicted in Figure 16 show that with WADC for BESS in candidate groups ρ_4 and ρ_9, the SG rotor oscillation, power oscillation in the inter-area line, BESS power oscillation, and d-axis reference current of the VSC for BESS are effectively damped. However, under the system operating condition γ_{p1}, these oscillations have slightly longer settling times than Scenarios S1 and S2. The proposed WADC damping performance outperforms the BESS-based WAPSS[25] regarding variable communication time delay uncertainty.

6.4 | Scenario 4 (S4)

This scenario integrates a solar photovoltaic (PV) system into the modified IEEE 39 bus system. The solar PV system, with a power capacity of 50 MW, is placed randomly on Bus 20 of the study system, as depicted in Figure 17. In this simulation scenario, the solar PV system is configured with 115 solar cells connected in series and 8,200 solar cells connected in parallel. Each solar cell operates at its maximum power point condition, generating 17.4 V voltage and 3.05 A current, thus achieving the desired power capacity for the solar PV system. Moreover, under this scenario, the solar PV system is simulated with solar irradiances fixed at 1,000 W/m^2 while maintaining a consistent temperature of 25°C throughout the analysis.

The dynamic simulation response of rotor speed deviation between SGs 4 and 2 and active power across the inter-area line using WADC for BESS in candidate groups ρ_4 are depicted in Figure 18A,B, respectively. These dynamic responses reveal that the proposed WADC provides superior damping performance compared to BESS-based WPSS,[25] effectively mitigating the rotor oscillations as well as power oscillation through the inter-area line. The increased settling time of SG rotor oscillations in Scenario S4 compared to Scenarios S1–S3 under operating condition γ_{p1} can be attributed to the lower inertia of converter-based resources compared to conventional generators. Additionally, solar PV systems provide less inherent damping, leading to a sluggish response to disturbances. Consequently, this leads to longer settling times for rotor speed oscillation.

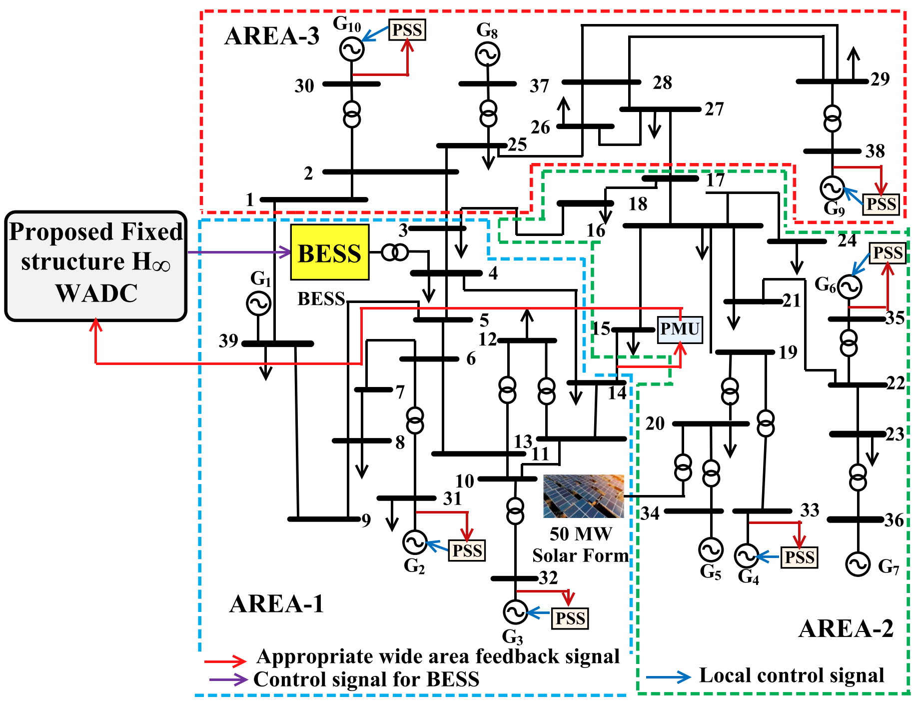

FIGURE 17 Modified IEEE 39 bus system with WADC for BESS and integrated solar PV system on Bus 20

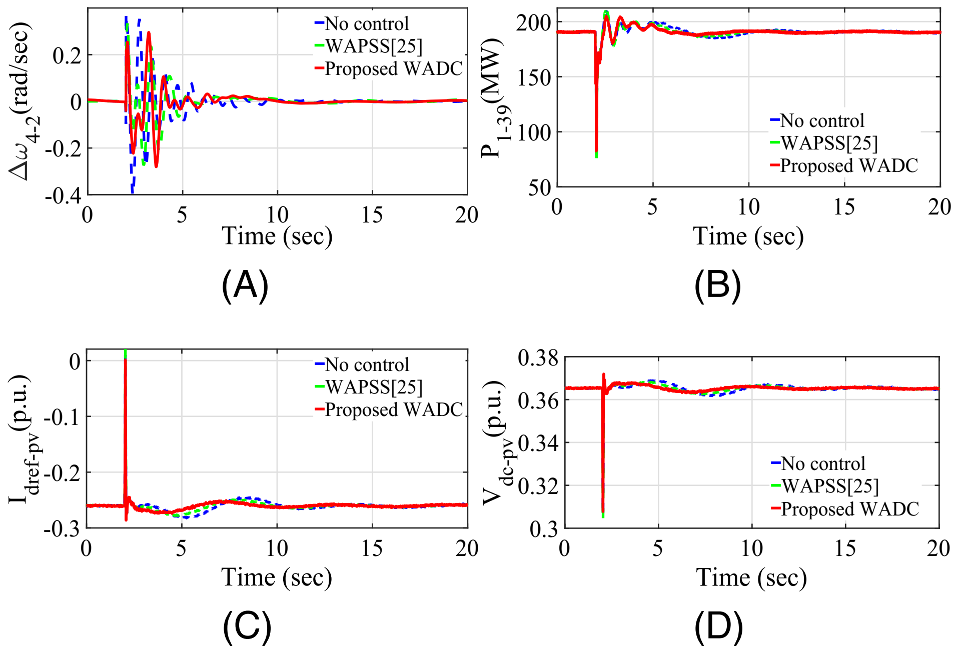

FIGURE 18 Dynamic response of the studied system integrating BESS and a PV system under operating condition γ_{p1} with WADC for BESS in candidate group ρ_4: (A) $\Delta\omega_{4-2}$, (B) P_{1-39}, (C) $I_{dref-PV}$ of GSC in PV system, and (D) V_{dc-PV} of PV system

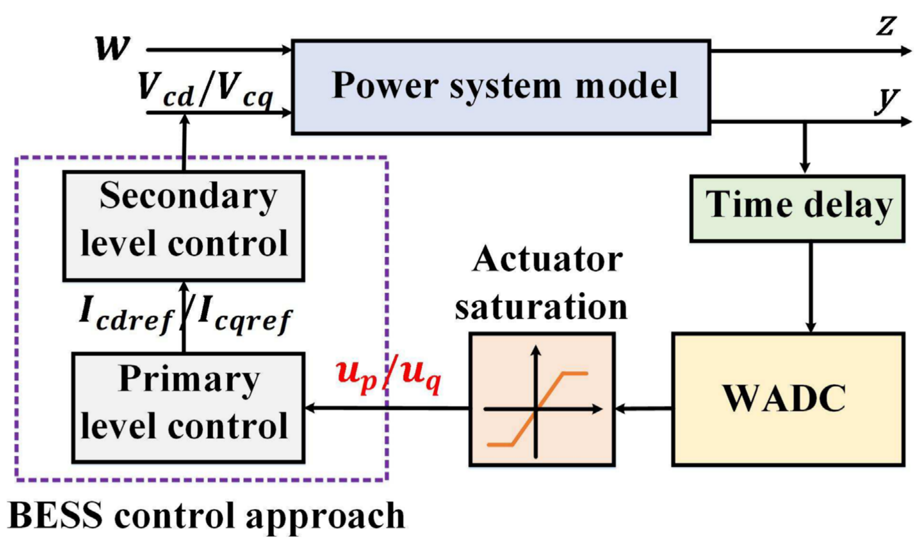

FIGURE 19 WADC with nonlinearity for BESS

Further dynamic responses of the d-axis reference current of grid-side VSC and DC-link voltage between the boost converter and grid-side converter are depicted in Figure 18C,D, respectively. These dynamic responses elucidate that the settling time and peak overshoot in the d-axis reference current of the grid-side VSC and the DC-link voltage between the boost converter and the grid-side converter are adequately damped subsequent to a severe contingency in Scenario S4. As a result, it is evident that the proposed WADC offers effective damping compared to the WAPSS[25] control scheme in a renewable integration scenario.

The dynamic simulations performed under different Scenarios (S1 to S4) confirm the efficacy of the proposed fixed-structure H_∞ WADC for BESS. This control approach demonstrates robust damping performance across various contingencies, encompassing varied system operating conditions, different fault types and locations, uncertainties associated with constant and variable communication time delays in the feedback loop, and integrating renewable sources.

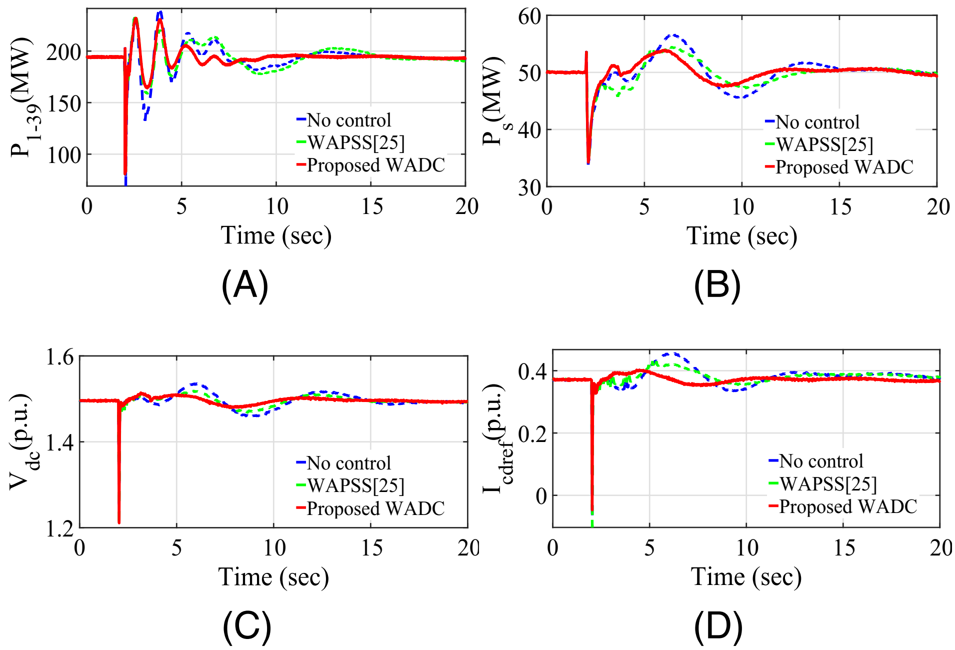

FIGURE 20 Dynamic response of the study system with a WADC linked with nonlinearity for BESS in candidate ρ_4 under operating condition γ_{p1}: (A) P_{1-39}, (B) P_s, (C) V_{dc}, and (D) I_{cdref}

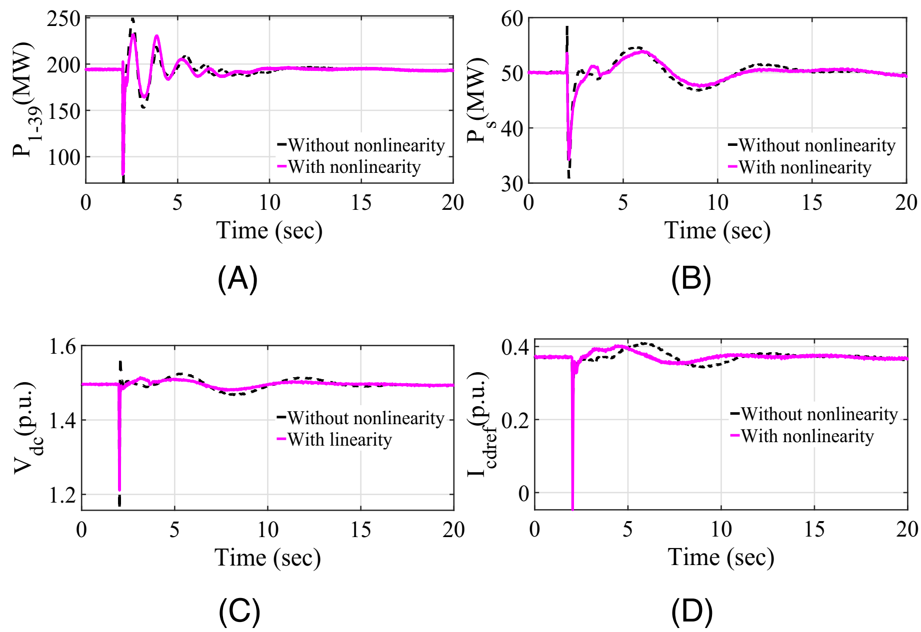

FIGURE 21 Dynamic response of the study system with a WADC linked without and with nonlinearity for BESS in candidate ρ_4 under operating condition γ_{p1}: (A) P_{1-39}, (B) P_s, (C) V_{dc}, and (D) I_{cdref}

6.5 | Effect of nonlinearity on proposed WADC for BESS

The proposed WADC for BESS includes nonlinearity, such as actuator saturation of output of the damping controller, as shown in Figure 19. The impact of system damping performance, including nonlinearity on the damping controller, is discussed in Maddela and Subudhi.[31]

In this simulation case, the actuator saturation limit, characterized by a nonlinear gain function, is applied to the output of the proposed WADC for BESS in candidate group ρ_4. This saturation limit includes a lower gain of 0.5, an input threshold value of 0.1, and an upper gain of 2. In this case, a three-phase fault is applied on the transmission line between Buses 16 and 19 at 3 s for 100 ms, and the study system is simulated under operating condition γ_{p1}.

The simulation responses of the study system, such as the power flow through inter-area line P_{1-39}, the active power of the BESS, the DC link voltage between the DC-DC bidirectional converter and the VSC of the BESS, and the d-axis reference current for the VSC of the BESS, are shown in Figure 20A–D, respectively. These results demonstrate that the oscillations occurring after a severe disturbance in the system are reduced compared to the WAPSS suggested in.[25] Additionally, the simulation response of the study system with the proposed WADC for the BESS, including with and without nonlinearity, is depicted in Figure 21. From this simulation response, it is observed that the WADC with nonlinearity effectively reduces the peak amplitude of oscillations in the inter-area line power flow, the output power of the BESS, the DC link voltage of the VSC of the BESS, and the VSC current of the BESS, providing superior damping performance compared to the WADC without nonlinearity. Consequently, the presence of nonlinearity in the damping controller notably reduces the system's oscillation response, enhances its overall damping performance, and prevents excessive control actions during severe disturbances.

7 | CONCLUSION

In this study, a fixed-structure H_∞ scheme-based WADC is designed for the BESS integrated power system. The location for installing BESS and the appropriate damping control loops, such as feedback signal and control loop (i.e., an active or reactive loop of BESS) to link the damping controller, are identified using the maximal of all minimal residues indices under various operating conditions of the system. This study unveils that the BESS active power control loop exhibits superior damping performance compared to the reactive power control loop in mitigating dominant inter-area oscillations under varying system operating conditions. The superiority of the proposed controller is confirmed by comparing the proposed WADC to the fixed-structure H_∞ WADC placed in the reactive power control loop, as well as a BESS-based WAPSS linked into active and reactive power control loops. The proposed fixed-structure H_∞ WADC is implemented in RTDS to assess its viability in a real-time environment. The outcomes of dynamic simulation and small-signal analysis validate the effectiveness of the proposed WADC in a multi-machine power system and are found to be superior.

Regarding the future aspect, the proposed design methodology encompasses packet drop considerations for remote data transfer and can address cybersecurity challenges in power system networks. Furthermore, a robust centralized mixed H_2/H_∞ control scheme could be designed for multiple BESS.

DATA AVAILABILITY STATEMENT

The data that support the findings of this study are available on request from the corresponding author. The data are not publicly available due to privacy or ethical restrictions.

ORCID

Rohit Kumar https://orcid.org/0000-0001-7919-0078
Mitresh Kumar Verma https://orcid.org/0000-0001-8323-6585

REFERENCES

1. Kundur P. *Power System Stability and Control*. McGraw-Hill; 1994.
2. Liu W, Venayagamoorthy GK, Wunsch DC. A heuristic-dynamic-programming-based power system stabilizer for a turbogenerator in a single-machine power system. *IEEE Trans. Ind. Appl.* 2005;41(5):1377-1385. doi:10.1109/TIA.2005.853386
3. Li M, Chen Y. A wide-area dynamic damping controller based on robust H_∞ control for wide-area power systems with random delay and packet dropout. *IEEE Trans. Power. Syst.* 2017;33(4):4026-4037.
4. Rangi S, Jain S, Arya Y. Utilization of energy storage devices with optimal controller for multi-area hydro-hydro power system under deregulated environment. *Sustain Energy Technol Assess*. 2022;52:102191. doi:10.1016/j.seta.2022.102191
5. Prakash T, Singh VP, Mohanty SR. A synchrophasor measurement based wide-area power system stabilizer design for inter-area oscillation damping considering variable time-delays. *Int. J. Elec. Power*. 2019;105:131-141. doi:10.1016/j.ijepes.2018.08.014
6. Bento ME. A hybrid particle swarm optimization algorithm for the wide-area damping control design. *IEEE Trans. Industr. Inform.* 2021;18(1):592-599. doi:10.1109/TII.2021.3054846
7. Beiraghi M, Ranjbar A. Adaptive delay compensator for the robust wide-area damping controller design. *IEEE Trans. Power. Syst.* 2016; 31(6):4966-4976. doi:10.1109/TPWRS.2016.2520397

8. Paternina MRA, Castrillón-Franco C, Zamora-Mendez A, et al. Enhancing wide-area damping controllers via data-assisted power system linear models. *Electr. Pow. Syst. Res.* 2023;217:109085. doi:10.1016/j.epsr.2022.109085
9. Kumar A, Bhadu M. Wide-area damping control system for large wind generation with multiple operational uncertainty. *Electr. Pow. Syst. Res.* 2022;213:108755. doi:10.1016/j.epsr.2022.108755
10. Alghamdi S, Markovic U, Stanojev O, Schiffer J, Hug G, Aristidou P. Wide-area oscillation damping in low-inertia grids under time-varying communication delays. *Electr. Pow. Syst. Res.* 2020;189:106629. doi:10.1016/j.epsr.2020.106629
11. Naguru NR. Design of a decentralized wide-area control system to tolerate the loss of communication paths based on coherency analysis. *Electr. Pow. Syst. Res.* 2023;222:109500. doi:10.1016/j.epsr.2023.109500
12. Thakallapelli A, Kamalasadan S. Alternating direction method of multipliers (ADMMS) based distributed approach for wide-area control. *IEEE Trans. Ind. Appl.* 2019;55(3):3215-3227. doi:10.1109/TIA.2019.2896837
13. Zenelis I, Wang X. A model-free sparse wide-area damping controller for inter-area oscillations. *Int. J. Elec. Power*. 2022;136:107609. doi:10.1016/j.ijepes.2021.107609
14. Kumar K, Prakash A, Singh P, Parida S. Large-scale solar PV converter based robust wide-area damping controller for critical low frequency oscillations in power systems. *IEEE Trans. Ind. Appl.* 2023;1-12. doi:10.1109/TIA.2023.3268632
15. Banerjee A, Chaudhuri NR, Kavasseri RG. A novel explicit disturbance model-based robust damping of interarea oscillations through MTDC grids embedded in ac systems. *IEEE Trans. Power Deliv.* 2018;33(4):1864-1874. doi:10.1109/TPWRD.2018.2799170
16. Zhu Y, Liu C, Sun K, Shi D, Wang Z. Optimization of battery energy storage to improve power system oscillation damping. *IEEE Trans. Sustain. Energy*. 2018;10(3):1015-1024.
17. Choudhary R, Rai J, Arya Y. Foptid+ 1 controller with capacitive energy storage for AGC performance enrichment of multi-source electric power systems. *Electr. Pow. Syst. Res.* 2023;221:109450. doi:10.1016/j.epsr.2023.109450
18. Zhao Y, Yao W, Zhang C-K, Ai X, Wen J. Resilient wide-area damping control to mitigate strong cyber attack: a multiple-controller switching approach. *IEEE Trans. Smart Grid*. 2022;14(3):2326-2337.
19. Calero F, Cañizares CA, Bhattacharya K. Dynamic modeling of battery energy storage and applications in transmission systems. *IEEE Trans. Smart Grid*. 2020;12(1):589-598. doi:10.1109/TSG.2020.3016298
20. Datta U, Kalam A, Shi J. Battery energy storage system to stabilize transient voltage and frequency and enhance power export capability. *IEEE Trans. Power. Syst.* 2018;34(3):1845-1857.
21. Bazargan D, Filizadeh S, Gole AM. Stability analysis of converter-connected battery energy storage systems in the grid. *IEEE Trans. Sustain. Energy*. 2014;5(4):1204-1212. doi:10.1109/TSTE.2014.2337053
22. Sun J, Mitchell DM, Greuel MF, Krein PT, Bass RM. Averaged modeling of PWM converters operating in discontinuous conduction mode. *IEEE Trans. Power Electron.* 2001;16(4):482-492. doi:10.1109/63.931052
23. Wu B, Lang Y, Zargari N, Kouro S. *Power Conversion and Control of Wind Energy Systems*. John Wiley & Sons; 2011. doi:10.1002/9781118029008
24. Bento ME. Fixed low-order wide-area damping controller considering time delays and power system operation uncertainties. *IEEE Trans. Power. Syst.* 2020;35(5):3918-3926. doi:10.1109/TPWRS.2020.2978426
25. Qi J, Wu Q, Zhang Y, Weng G, Zhou D. Unified residue method for design of compact wide-area damping controller based on power system stabilizer. *J. Mod. Power Syst. Clean Energy*. 2020;8(2):367-376. doi:10.35833/MPCE.2018.000370
26. Wang H. Selection of robust installing locations and feedback signals of facts-based stabilizers in multi-machine power systems. *IEEE Trans. Power. Syst.* 1999;14(2):569-574. doi:10.1109/59.761882
27. Skogestad S, Postlethwaite I. *Multivariable Feedback Control: Analysis and Design*. John Wiley & Sons; 2005.
28. Apkarian P, Noll D. Nonsmooth H_∞ synthesis. *IEEE Trans. Automat. Contr.* 2006;51(1):71-86.
29. Yao W, Jiang L, Wen J, Wu Q, Cheng S. Wide-area damping controller of facts devices for inter-area oscillations considering communication time delays. *IEEE Trans. Power. Syst.* 2013;29(1):318-329. doi:10.1109/TPWRS.2013.2280216
30. Hiskens I. "IEEE PES task force on benchmark systems for stability controls," Technical report, 2013.
31. Maddela CO, Subudhi B. Robust wide-area TCSC controller for damping enhancement of inter-area oscillations in an interconnected power system with actuator saturation. *IJEPES*. 2019;105:478-487. doi:10.1016/j.ijepes.2018.08.042

How to cite this article: Kumar R, Mohanty SR, Verma MK. Enhancing damping of low-frequency oscillations in power networks through energy storage system-based controller. *Int J Circ Theor Appl*. 2025;53(4):2292-2317. doi:10.1002/cta.4196